

Effective one-dimension reduction of multi-compartment complex systems dynamics

Giorgio Vittorio Visco,^{1,*} Oriol Artime,^{2,3,4} Johannes Nauta,¹ Tomas Scagliarini,¹ and Manlio De Domenico^{1,5,6,†}

¹*Department of Physics and Astronomy “Galileo Galilei”,
University of Padua, Via F. Marzolo 8, 315126 Padova, Italy*

²*Departament de Física de la Matèria Condensada,
Universitat de Barcelona, 08028 Barcelona, Spain*

³*University of Barcelona Institute of Complex Systems (UBICS),
Universitat de Barcelona, 08028 Barcelona, Spain*

⁴*Universitat de les Illes Balears, 07122 Palma, Spain*

⁵*Padua Center for Network Medicine, University of Padua, Via F. Marzolo 8, 315126 Padova, Italy*

⁶*Istituto Nazionale di Fisica Nucleare, Sez. Padova, Italy*

(Dated: April 18, 2024)

A broad class of systems, including ecological, epidemiological, and sociological ones, are characterized by populations of individuals assigned to specific categories, e.g., a chemical species, an opinion or an epidemic state, that are modeled as compartments. Due to interactions and intrinsic dynamics, individuals are allowed to change category, leading to concentrations varying over time with complex behavior, typical of reaction-diffusion systems. While compartmental modeling provides a powerful framework for studying the dynamics of such populations and describe the spatiotemporal evolution of a system, it mostly relies on deterministic mean-field descriptions to deal with systems with many degrees of freedom. Here, we propose a method to alleviate some of the limitations of compartmental models by capitalizing on tools originating from quantum physics to systematically reduce multi-dimensional systems to an effective one-dimensional representation. Using this reduced system, we are able to not only investigate the mean-field dynamics and their critical behavior, but we can additionally study stochastic representations that capture fundamental features of the system. We demonstrate the validity of our formalism by studying the critical behavior of models widely adopted to study epidemic, ecological and economic systems.

I. INTRODUCTION

Complex systems consist of a multitude of interconnected and interacting entities that form extensive networks, with typical examples ranging from chemical to ecological and social ones [1–9]. To analyze their complex behavior, often characterized by collective dynamics, phase transitions and other emergent phenomena, compartmental modeling is usually adopted. In this framework, units of the system are categorized or stratified into distinct species, states or categories, referred to as compartments, and the concentration of units in each compartment is studied over time while taking into account the change of species due to either unit-unit interactions or spontaneous transitions into other compartments.

Compartmentalization facilitates the study of dynamic behaviors and phase transitions in some order parameters as a function of control parameters that directly depend on modeling assumptions and observables. For instance, in the case of an epidemic outbreak it is possible to study how the steady-state density of infected individuals depends on the transmission rate of a pathogen by means of social contacts and the recovery rate from the corresponding disease [10–12] (see [13] for an extensive review). One of the most successful frameworks to study the behavior of such epidemic systems, as well as of the

ones consisting of multiple interconnected compartments, is based on the study of the next-generation matrix, an indispensable tool for analyzing the conditions required to favor the emergence of active states where epidemics dynamics is sustained and infection has the potential to scale at system level [14, 15].

Despite its successes, compartmental modeling comes with some limitations. For instance, the aforementioned next-generation matrix formalism, while robust, offers a limited scope in addressing the multitude of degrees of freedom present in large-scale interconnected systems. In fact, the presence of this constraint requires the introduction of simplifying assumptions and approximations, often in the form of deterministic mean-field equations, to deal with the complexity inherent in these systems. Nevertheless, these approximations can be still very powerful: for example, in the case of complex networks with an heterogeneous degree distribution it is possible to consider classes of a specific degree and then study the dynamics of the overall system by means of the dynamics of such classes. This approach leads to heterogeneous mean-field equations that allows one to model the collective behavior of a system more accurately than simple homogeneous mean-field equations [16–18].

In fact, this approach shares commonalities with the study of the broad class of reaction-diffusion processes to describe chemical reaction networks [19], where units are chemical species undergoing transitions because of chemical reactions or spontaneous transformations. This parallel is striking and it is therefore natural to wonder if, and under which conditions, it is possible to analyze

* giorgiovittorio.visco@phd.unipd.it

† manlio.dedomenico@unipd.it

population dynamics of a variety of complex systems by means of a formalism that overcomes the inherent limitations of the current ones.

Chemical reaction networks (broadly speaking) have been extensively studied by means of the Doi-Peliti formalism [20, 21], offering a rich methodology for analyzing both stochastic and deterministic dynamics beyond pure mean-field approaches. However, while chemical reaction networks are subject to strict constraints, such as the mass balance of chemical elements [22, 23], this is not always the case for the general systems we are interested in in this work, where compartments can also be of heterogeneous nature. Therefore, we anticipate that it will be necessary to adapt the Doi-Peliti formalism to deal with the variety of cases of interest for network and complexity science. Accordingly, in the following, we will refer in general to chemical reaction networks (CRNs) to indicate such a broad spectrum of systems, from chemical to ecological and social ones.

The dynamics of a CRN can be completely described by a master equation and the Doi-Peliti formalism recalls the second quantization used in quantum field theory to apply the methods for studying quantum systems for the analysis of stochastic classical systems. One of these methods is the path integral representation [24], that is particularly useful to go beyond the deterministic mean-field limit of a model, providing insights on its stochastic behavior. In the last years, attempts to extend this formalism to systems with many degrees of freedom have been proposed [24–27], although providing general results is still a challenging endeavour.

Building upon these works, we develop a framework that describes multi-compartment systems by reducing them to a one-dimensional effective model, showing how to map a CRN to a Hamiltonian problem. This mapping allows us to characterize the critical behavior, if any, of the CRN through an elegant geometrical interpretation. Furthermore, irrespectively of the presence, or lack thereof, of phase transitions in the stochastic process of interest, our formalism provides a way to approximate its steady-state with high accuracy even for systems where existing approaches cannot be readily used. The idea of building on methods originating from quantum physics to study complex networks, or viceversa, has proven successful to stretch the boundaries of statistical physics [28–36]. Similarly, we foresee broad applications of our dimensionality reduction approach to study the critical behaviour and the population dynamics of multi-compartment processes.

The article is organized as follows. We first provide the theoretical basis of our work in Sec. II, where we introduce the terminology, discuss the Doi-Peliti’s path integral formalism for the study of CRNs, and lay out the mapping from CRNs to Hamiltonian systems. In Sec. III, we present the geometrical interpretation of phase transitions by means of the analysis of phase portraits, and detail how to classify them. In Sec. IV, we present the method for dimensionality reduction to an effective one-

dimensional model for the dynamics. Throughout the article, we accompany the theoretical results with applications to stochastic models of different nature and increasing complexity, thus validating our framework and discussing its limitations. We close the article with our conclusions in Sec. V.

II. THEORETICAL BACKGROUND

A. Stochastic compartmental models

Many natural, biological and socio-technical phenomena can be modelled by means of stochastic processes. Through a probabilistic representation, one focuses on a macroscopic quantity n whose dynamics is probabilistically described by a distribution $p(n, t)$ that depends on the features of the system. Some examples include the disease spreading, where n represents the number of infected individuals, or ecological systems where this variable describes species abundance. From a mathematical point of view, n is the output of a discrete random variable, whereas $p(n, t)$ is the probability of finding that random variable with value n at time t . Generally, we can take n as a discrete quantity. We will focus on homogeneous Markovian systems only, therefore the dynamical behaviour of the systems is governed by a master equation

$$\partial_t p(n, t) = \sum_m H_{nm} p(m, t), \quad (1)$$

where the sum is evaluated over all possible states, and H_{nm} elements of a matrix that is defined by the system interactions. This matrix can be written in terms of the transition rates $\omega(n|m)$, that represent the probability per unit of time of transitioning from the state m to the state n , that is

$$H_{nm} = \omega(n|m) - \delta_{n,m} \sum_{m'} \omega(m'|n), \quad (2)$$

where δ_{nm} is the Kronecker delta. This compartmental representation is very flexible, and the evolution of the system narrows down to keeping trace of the number of elements that belong to each state-compartment.

Now let M be the number of compartments necessary to fully characterize a system, which we denote $\{I_i\}_{i=1, \dots, M}$. In this case, $\mathbf{n} = (n_1, n_2, \dots, n_M)$ is the (multi-dimensional) variable of interest, and n_i is the population number in the i -th compartment. For a generic system, M can be arbitrarily large, and the interaction network very complex. For the sake of simplicity, in this work we limit ourselves to the case of well-mixed reaction networks, given by the set of transitions

$$\sum_{i=1}^M A_i I_i \rightarrow \sum_{i=1}^M B_i I_i. \quad (3)$$

where $\{A_i, B_i\}_{i=1, \dots, M}$ represent the stoichiometric coefficients [27]. Note that these are mass-action reactions, meaning that the rates are proportional to the population numbers.

Next we will provide methods to study systems fulfilling these transitions. We will show that our proposed formalism will simplify the analysis of these systems by focusing only on the effective dynamics of a single compartment. Before introducing our formalism, let us first present the path integral formulation and its relation to classical Hamiltonian systems.

B. The Doi-Peliti formalism and the path integral representation

A useful tool to handle CRNs is the Doi-Peliti (DP) formalism [20, 21]. This formalism describes the dynamics of a population using creation and annihilation operators, denoted by a^\dagger and a respectively. Thus, analogous with second quantization, an element of the system can be created or destroyed following the prescriptions of the ME. This approach has been extensively covered in the literature (see, e.g., Ref. [24]). While there are several ways one can introduce the main components of the formalism, we adhere to the standard definition and develop the usual path integral representation [21, 24, 27, 37].

We proceed by noting that we use Dirac's bracket notation to describe the state of a system, i.e. $|\mathbf{n}\rangle = |n_1, n_2, \dots, n_M\rangle$. The corresponding bra is given by the normalization condition

$$\langle \mathbf{n} | \mathbf{n}' \rangle = \prod_{i=1}^M n_i! \delta_{n_i n'_i}. \quad (4)$$

With this normalization condition, the creating and annihilation operators are defined by

$$a_i^\dagger |\mathbf{n}\rangle = |\mathbf{n} + \mathbb{I}_i\rangle, \quad a_i |\mathbf{n}\rangle = n_i |\mathbf{n} - \mathbb{I}_i\rangle, \quad (5)$$

where \mathbb{I}_i is the canonical vector with the i -th component equal to 1 and all others zero. Thus, within the context of compartmental models, a_i^\dagger and a_i respectively create and annihilate an element belonging to compartment I_i respectively, and follow the usual bosonic commutation relation. To arrive at a path integral representation, let us introduce the generating function

$$|G\rangle = \sum_{\mathbf{n}} p(\mathbf{n}, t) |\mathbf{n}\rangle, \quad (6)$$

and, by using Eq. (4), the probability distribution of attaining a specific state at time t reads

$$p(\mathbf{n}, t) = \frac{\langle \mathbf{n} | G \rangle}{\prod_i n_i!}.$$

Thus, $|G\rangle$ fully determines the statistical behaviour of the system. By employing the ME (Eq. (1)), we obtain

a ‘‘Schrödinger-like’’ equation within the Doi-Peliti representation, which reads

$$\partial_t |G\rangle = \mathcal{H} |G\rangle, \quad (7)$$

where

$$\mathcal{H} = \sum_{\mathbf{n}, \mathbf{m}} \frac{1}{\prod_i m_i!} |\mathbf{n}\rangle H_{nm} \langle \mathbf{m}| \quad (8)$$

is the *Doi-Peliti Hamiltonian* (DPH). For a CRN, the DPH can be written as a polynomial function of the creation and annihilation operators (Appendix D).

As a basis for the Fock space, we work with

$$|\mathbf{n}\rangle = \prod_{i=1}^M x_i^{n_i}, \quad (9)$$

where $\mathbf{x} = (x_1, \dots, x_M) \in \mathbb{R}^M$. Hence, using the normalization condition, we have that

$$\langle \mathbf{n} | = \prod \left(\frac{\partial}{\partial x_i} \right)^{n_i} \Big|_{\mathbf{x}=0} \quad (10)$$

Under these bases, the path-integral representation for the generating function is given by [24]

$$|G\rangle = \int_0^t \mathcal{D}[\mathbf{x}, \mathbf{q}] e^{-\mathcal{S}[\mathbf{x}, \mathbf{q}] + \sum_j n_{0j} \log x_{0j}}, \quad (11)$$

where i the imaginary unit, \mathbf{n}_0 is the initial state of the stochastic process, $\mathcal{D}[\mathbf{x}, \mathbf{q}]$ a suitable measure [24, 37], and \mathcal{S} is the action of the system defined as (Appendix A)

$$\mathcal{S}[\mathbf{x}, \mathbf{q}] = - \int_0^t d\tau \left[\sum_j i q_j(\tau) \partial_\tau x_j(\tau) + \mathcal{H}(\mathbf{x}(\tau), \mathbf{i}q(\tau)) \right] \quad (12)$$

Within the path integral representation, the operators a_j^\dagger and a_j are replaced by two fields $x_j(\tau)$ and $i q_j(\tau)$. They are linked to the random variable through the formal relation $i q_j x_j = n_j$, which comes from the definition of the number operators $\hat{N}_j = a_j^\dagger a_j$ ($\hat{N}_j |\mathbf{n}\rangle = n_j |\mathbf{n}\rangle$). Note that handling Eq. (11) is generally difficult, but in the case of chemical reactions, we will show that we can an approximation similar to the Wentzel-Kramers-Brillouin (WKB) in spirit, reducing the study of a stochastic process to a Hamiltonian problem.

C. Stationary paths and Hamiltonian systems

The path integral representation is formally exact, but to obtain explicit results one has to resort to approximations. Recently, it has been shown that the WKB approximation for the study of stochastic systems is a good candidate [26, 38–40]. In Appendix B we prove this approximation can be applied to CRNs as those in Eq. (3),

thus greatly simplifying the path integral representation. Using this approximation, the generating function can be approximated by $\langle G \rangle \approx \exp(-\mathcal{S})$ where \mathcal{S} here is the stationary action. Thus, the principal contributors inside the integration of Eq. (6) are the solutions $(\tilde{\mathbf{x}}, \tilde{\mathbf{q}})$ of the Hamilton-Jacobi equations with Hamiltonian $-\mathcal{H}$;

$$\frac{\partial \tilde{\mathbf{x}}}{\partial t} = -\frac{\partial \mathcal{H}}{\partial \tilde{\mathbf{q}}}, \quad \frac{\partial \tilde{\mathbf{q}}}{\partial t} = \frac{\partial \mathcal{H}}{\partial \tilde{\mathbf{x}}}. \quad (13)$$

While this system of equations might seem complicated, it represents an alternative description to the ME, and, as we will see, valuable information about the dynamical properties of the stochastic process can be extracted from it.

As we work with chemical reactions where the WKB approximation holds, we will consider only stationary trajectories denoted with \mathbf{x} and \mathbf{q} . In Appendix C, we show that the stationary trajectories can be taken as real positive functions satisfying the relation $x_j q_j = n_j$.

Note that the trajectory $x_j = 1$ is a solution of Eq. (13). It plays an important role from a statistical point of view. Indeed, by our definitions, the average value of n_j is given by

$$\langle n_j \rangle = \left. \frac{\partial \langle G \rangle}{\partial x_j} \right|_{\mathbf{x}=1} = q_j, \quad (14)$$

where we have used the Hamilton-Jacobi relations. Thus, in the phase space, the deterministic behaviour (i.e. the mean-field behavior) of the system is contained on the mean-field manifold $\mathbf{x} = 1$. As we will illustrate, this manifold is key in the analysis of the phase transitions on the phase portrait of the system.

III. PHASE PORTRAITS AND PHASE TRANSITIONS

So far we have used the Doi-Peliti formalism to map the dynamics of a CRN to a Hamiltonian system through two vectors that encode the dynamics of the process \mathbf{x} and \mathbf{iq} . To provide a clearer physical interpretation of our variables, we use the Cole-Hopf (CH) transformation [41]

$$x_j = e^{i\theta_j}, \quad q_j = \eta_j e^{-i\theta_j}, \quad (15)$$

with $\eta_j, \theta_j \in \mathbb{R}$. In doing so, we replace the field $(\mathbf{n}, \mathbf{iq})$ with $(\boldsymbol{\eta}, \mathbf{i}\boldsymbol{\theta})$, where now η_j represents the population number n_j . With these variables, the action \mathcal{S} becomes

$$\mathcal{S} = \int_{t_0}^t d\tau \left[\sum_j i\theta_j \partial_\tau \eta_j - \mathcal{H}(e^{i\boldsymbol{\theta}}, \boldsymbol{\eta} e^{-i\boldsymbol{\theta}}) \right] + i\boldsymbol{\theta}(t_0)\boldsymbol{\eta}(t_0) - i\boldsymbol{\theta}(t)\boldsymbol{\eta}(t),$$

and the system of Eq. (13) reads

$$\begin{aligned} \frac{\partial \boldsymbol{\eta}}{\partial t} &= -i \frac{\partial}{\partial \boldsymbol{\theta}} \mathcal{H}(e^{i\boldsymbol{\theta}}, \boldsymbol{\eta} e^{-i\boldsymbol{\theta}}) \\ i \frac{\partial \boldsymbol{\theta}}{\partial t} &= -\frac{\partial}{\partial \boldsymbol{\eta}} \mathcal{H}(e^{i\boldsymbol{\theta}}, \boldsymbol{\eta} e^{-i\boldsymbol{\theta}}) \end{aligned} \quad (16)$$

Note that mean-field manifold $\mathbf{x} = 1$ ($\boldsymbol{\theta} = 0$) is always a solution of both Eqs. (13) and (16). Thus, it is a universal feature of CRNs, as discussed in [42]. A more formal proof of this property is provided in Appendix D.

As it has been done for $(\mathbf{x}, \mathbf{iq})$, in the stationary limit we replace $(\boldsymbol{\eta}, \mathbf{i}\boldsymbol{\theta})$ with the (real) solutions of (16). With this change of coordinates, the mean-field dynamics is recovered on $\boldsymbol{\theta} = 0$. Thus, the physical interpretation of $\boldsymbol{\theta}$ relates to how much the dynamical behaviour of the system is close to the deterministic one. In other words, $\boldsymbol{\theta}$ expresses the role of the stochastic fluctuations *beyond* the mean-field approximation. Therefore, by studying the phase portrait of (16), we can investigate the time evolution through its attractors. Moreover, we are able to probe the role of fluctuations, which shall be discussed in Section III B.

Note that while presented transformation offers a clearer interpretation of the fields representing the creation and the annihilation operators, it implies technical difficulties as well, as shall be illustrated below. In the following sections, we will alternate between the (\mathbf{x}, \mathbf{q}) representation and the Cole-Hopf $(\boldsymbol{\eta}, \boldsymbol{\theta})$ one, showing that the former tends to be more suitable for analytic computations, while the latter is more convenient for graphical visualizations of the phase portraits.

A. The Doi-Peliti formalism and the characterization of phase transitions

Following ideas put forward in [25], we build on the formalism presented so far to develop a mathematical framework for the analysis of phase transitions. In particular, our approach overcomes the limitations present when considering one-compartment models only, thus offering a tool for the analysis of the critical and stochastic behavior of general multidimensional compartmental model. We consider systems that converge to a steady state for $t \rightarrow \infty$. These systems are typically out of equilibrium, hence they cannot be treated with the tools of equilibrium statistical mechanics, such as the Landau theory [43]. The non-equilibrium properties, however, can be easily addressed by leveraging the Doi-Peliti mapping to the Hamiltonian representation.

We will describe our system by means of a non-equilibrium order parameter ρ , which denotes the asymptotic density of a specific compartment. We focus on cases in which the initial size of a compartment of a certain state I_1 is large. That is, $n_1 \approx N$, and hence

$$\rho = 1 - \lim_{t \rightarrow \infty} \frac{\langle n_1 \rangle}{N}. \quad (17)$$

Within the context of epidemiology, this means that the number of susceptible individuals dominates, and the study of the dynamics consists in observing how the system responds by inserting a small amount of infected individuals.

As we are interested in the large time behaviour, Eq. (7) hints towards focusing our attention on the zero-energy sets $\mathcal{H} = 0$. Within the WKB approximation, we are able to study the topology of these sets to obtain information about the system at large times. Here, by topology we mean the structure of the trajectories on the phase portrait related to \mathcal{H} . The fixed points of the Hamiltonian system on the manifold $\mathcal{H} = 0$ play an important role since they are related to the stable and the unstable manifold that determine the system's evolution [44]. In particular, the dynamics converges at the hyperbolic fixed point on the stable manifold, and diverges from it on the unstable one. Therefore, when modifying the control parameters, such as the coefficients of transition rates of the web of interactions among compartments, the configuration of the fixed points changes. As a result, the dynamics of the system will vary with its attractors, suggesting the presence of phase transitions. Moreover, as stated above, $\mathbf{x} = 1$ is the stationary trajectory for which $\mathcal{H} = 0$, and it represents the mean-field dynamics. By studying the fixed points on $\mathbf{x} = 1$, we can recover the mean-field phase transitions, and, by analysing the topology of the stable and unstable manifold, we are able to characterize these transitions [25]. If new fixed points appear when the control parameters are modified, then the dynamics of the system radically change, leading to first-order phase transition. Instead, if we observe that the number of fixed points does not vary but their positions change, then the asymptotic configuration continuously varies with respect to the control parameters and thus a second-order transition is present.

After these considerations, we define the following strategy for studying possible phase transitions for a multi-compartment system:

1. find the Doi-Peliti Hamiltonian of the system;
2. look for the fixed points on the zero-energy sets;
3. look for conditions at which the determinant of the system Jacobian is null;
4. find parameter relations that characterize the phase transition;

When looking for the zero-energy sets, one must take all possible constraints into account, such as conservation of the total number of elements. In doing so, the system will be reduced to a size $2M - 2m$, where m is the number of constraints (see below). The determinant of the Jacobian is null when the Jacobian has at least two null eigenvalues. And finally, by varying the (control) parameters near the critical point(s), we can determine whether there is a first- or second-order phase transition, as we described above.

Regarding the constraints, we represent these by an equation of the form $\mathbf{C} = \mathcal{C}(\mathbf{x}, \mathbf{q})$, where \mathbf{C} is now an m -dimensional vector. Assuming that the implicit function theorem holds, we carry out a function Q such that, for m components of \mathbf{q} , we have:

$$(q_1, \dots, q_m) = Q(q_{m+1}, \dots, q_M, x_1, \dots, x_M, \mathbf{C}). \quad (18)$$

Furthermore, constraints represent first integrals of the Hamiltonian system. By substituting Eq. (18) into the DPH, we obtain a Hamiltonian that is independent of these variables, therefore the time derivatives of the corresponding conjugate coordinates (x_1, \dots, x_m) are all zero, and thus we can let $x_i = 1$ for all $i = 1, \dots, m$. Each constraint reduces the dimension of the system by 2, projecting the DPH onto a new, reduced Hamiltonian \mathcal{H}^* that depends on $2M - 2m$ variables. Under these premises, the system reads

$$\partial_{x_j} \mathcal{H}^* = 0, \quad \partial_{q_j} \mathcal{H}^* = 0 \quad (19)$$

with the constraints

$$x_j = 1, \quad \det(\mathbf{J}) = 0, \quad (20)$$

where \mathbf{J} is the Jacobian of \mathcal{H}^* in terms of \mathbf{x} and \mathbf{q} . By treating the coefficients of the transition rates as variables, the system of Eq. (19) gives us the critical points for possible phase transitions. In the same way, we can build this system by using the Cole-Hopf coordinates.

In the following section we shall use the Cole-Hopf variables and show how to derive the Langevin dynamics starting from a generic DPH, and the accompanying Fokker-Planck equation for the corresponding probability distribution.

B. Fokker-Planck and Langevin representations

The Cole-Hopf variables allow us to represent the fluctuations around the mean-field dynamics by means of θ . We have seen that, from the first derivative of \mathcal{H}^* with respect to θ evaluated at zero, we get the dynamics of the reduced system. Now, we show that, from its second derivative, we can infer the behavior of the system due to fluctuations, as done in [24, 27].

Let us consider, for now, a single-compartment system and take the reduced Hamiltonian \mathcal{H}^* in the Cole-Hopf representation. When the population number n is sufficiently large, it can be approximated by a continuous variable. In doing so, we can re-write the ME of Eq. (1) using a Kramers-Moyal expansion [24],

$$\begin{aligned} \partial_t p(n, t) &= \sum_{m \geq 1} \frac{(-1)^m}{m!} \frac{\partial^m}{\partial n^m} [W_m(n) p(n, t)] \\ &= \mathcal{H}_{KM}(n, \partial_n) p(n, t), \end{aligned} \quad (21)$$

with

$$W_m(n) = \int_{\mathbb{R}} dy y^m \omega(n + y, n), \quad (22)$$

and where \mathcal{H}_{KM} the Kramers-Moyal operator. In this limit, a link between the Doi-Peliti Hamiltonian and \mathcal{H}_{KM} exists. Using the definition of \mathcal{H} , and considering Eq. (8), one can prove that for one-dimensional systems the following holds;

$$\mathcal{H}_{KM}^\dagger(\eta, \partial_\eta) = \mathcal{H}(\eta, \theta) \quad (23)$$

where \mathcal{H}_{KM}^\dagger is the adjoint operator of \mathcal{H}_{KM} . Under this mapping, we have $\eta = n$ and $\theta = \partial_n$.

The same reasoning can be applied to systems with more degrees of freedom by using the dimension reduction presented above. If we consider the average of $n_1 = \eta$ as the order parameter, by expanding \mathcal{H}^* up to the second-order of θ around $\theta = 0$, we then obtain a Fokker-Planck equation [45]

$$\partial_t p(\eta, t) = -\partial_\eta [\partial_\theta \mathcal{H}_0^* p(\eta, t)] + \partial_\eta^2 [\frac{1}{2} \partial_\theta^2 \mathcal{H}_0^* p(\eta, t)], \quad (24)$$

where, with some slight abuse of notation, we have $\partial_\theta^k \mathcal{H}_0^* = (\partial_\theta^k \mathcal{H}^*)|_{\theta=0}$ and $p(\eta, t)$ the conditional probability distribution constrained by the stationary conditions. Hence, by expanding the reduced Hamiltonian, we can write an effective one-dimensional Fokker-Planck equation for the multi-compartment stochastic process, that makes further calculations considerably easier. From the Fokker-Planck equation, we can readily obtain the Langevin equation of the problem [45]

$$\frac{d\eta}{dt} = \partial_\theta \mathcal{H}_0^* + \sqrt{\partial_\theta^2 \mathcal{H}_0^*} \xi(t) \quad (25)$$

with $\xi(t)$ Gaussian white noise. Formal steady-state solutions of Eq. (23) are known to be [46]

$$\lim_{t \rightarrow \infty} p(\eta, t) = \mathcal{Z} e^{-V(\eta)}, \quad (26)$$

with the potential

$$V(\eta) = \int d\eta \frac{\partial_\eta (\partial_\theta^2 \mathcal{H}_0^*) - 2\partial_\theta \mathcal{H}_0^*}{\partial_\theta^2 \mathcal{H}_0^*}, \quad (27)$$

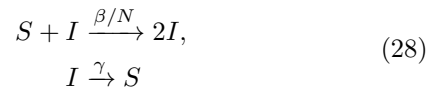
and \mathcal{Z} the normalization factor. Here it is clear that that $\partial_\theta^2 \mathcal{H}^*$ is related to the system's fluctuations and that, by employing the Doi-Peliti formalism, we can gather together both the deterministic and the stochastic dynamics.

Eqs. (19) and (25) constitute the grounds on which we will develop a framework adapted for the systematic study of multi-dimensional systems. Yet, we shall first show how to combine the results reported so far to handle models with two compartments. In Section III C, we treat a modified *SIS* model in which we inserted higher order interactions. We observe how the Doi-Peliti representation allows us to gain information on the critical behavior by unveiling tricritical points. In Sec. III D, we analyse phase transitions depending on the system initial configuration. Afterwards, we will then extend this approach to multi-dimensional problems by presenting a novel dimensional reduction method (Sec. IV A), which offer insights even in cases where other methods fail, as the well-known next-generation matrix [15]. Similarly, for illustrative purposes, we will showcase the implementation of this in models with interesting critical behavior: a modified *SIRS* model (Sec. IV B), two Lotka-Volterra models (Secs. IV C and IV C 2) and an exploiter-resource model IV D proposed by us. In addition, in Appendix F

we report further examples applied to several other contexts, such as tax evasion models. In Table I we summarise all the models treated in this paper with the main results.

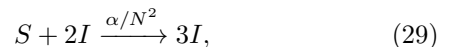
C. Application to epidemiology: A modified *SIS* model

Let us now analyse a modified Susceptible-Infected-Susceptible (SIS) model to illustrate our method. The SIS model is an epidemiological model that describes the interactions between elements of a population that are in either of two compartments; the susceptible S and the infected I compartments. Upon contact with an infected individual, a susceptible can become infected with rate β . Infected individuals recover from the disease with rate γ . The elementary reactions thus read



This system has been studied extensively and it is known that there is a continuous phase transition at $\beta = \gamma$ [13]. For $\beta > \gamma$, in the limit $t \rightarrow \infty$ the disease prevails in the population, impacting a macroscopic fraction of individuals, and so $\rho = 1 - \langle n_I \rangle / N > 0$. For $\beta < \gamma$, the disease will eventually disappear, and the system converges to the inactive (absorbing) phase. In general, for such epidemiological models, the initial condition is taken $n_S \approx N$, but obviously $n_S \leq N$.

To showcase the potential of this framework with respect to more traditional approaches, we include an additional reaction that underlies richer critical scenarios. More specifically, we consider an additive elementary reaction,



that corresponds to an additional transition rate,

$$\omega(\mathbf{n} - \mathbb{I}_S + \mathbb{I}_I, \mathbf{n}) = \alpha \frac{n_S n_I (n_I - 1)}{N^2}. \quad (30)$$

This is a three-body-like interaction that may interpreted as a process that helps the diffusion of the disease, mediated by the parameter α .

Taken all the rules together, the Doi-Peliti Hamiltonian reads

$$\begin{aligned} \mathcal{H} &= \frac{\alpha}{N^2} (a_I^\dagger)^2 (a_I^\dagger - a_S^\dagger) a_S a_I^2 \\ &+ \frac{\beta}{N} (a_I^\dagger - a_S^\dagger) a_I^\dagger a_I a_S \\ &+ \gamma (a_S^\dagger - a_I^\dagger) a_I, \end{aligned} \quad (31)$$

Model	# Compartments	# Constraints	Order Parameter	Critical Behavior
Modified <i>SIS</i> - 1	2	1	$1 - \langle n_S \rangle / N$	tricritical point
Modified <i>SIS</i> - 2	2	2	$1 - \langle n_S \rangle / N$	first order
Modified <i>SIRS</i>	3	1	$1 - \langle n_A \rangle / N$	tricritical point
Lotka-Volterra	2	0	$\langle n_N \rangle$	second order
Resource-Exploiters	3	0	$1 - \langle n_R \rangle / k_R$	second order
<i>SEIRS</i>	4	1	$1 - \langle n_S \rangle / N$	second order
<i>SEIR</i> with $E_{1,2}$	5	1	$1 - \langle n_S \rangle / N$	second order
Tax evasion	3	1	$1 - \langle n_H \rangle / N$	tricritical point
Levin	3	1	$1 - \langle n_A \rangle / N$	multiple phases

Table I: Models studied with the Doi-Peliti representation, in order of appearance in the article. For each model, we report the number of compartment and constraints, the compartment related to the order parameter, with its average taken at the stationary limit $t \rightarrow \infty$, and the type of phase transition identified with our approach. The Modified *SIS* models are treated in Sec. III C, the Modified *SIRS* model in Sec. IV B, the Lotka-Volterra model in Sec. IV C and the Resource-Exploiters model in Sec. IV D. In the Appendix, we address the *SEIRS* model in Sec. F 1, the *SEIR* model with latent categories $E_{1,2}$ in Sec. F 2, the Tax evasion model in Sec. F 3 and the Levin model in Sec. F 4.

and the corresponding mean-field trajectories read

$$\frac{\partial \langle n_S \rangle}{\partial t} = \gamma \langle n_I \rangle - \frac{\beta}{N} \langle n_S \rangle \langle n_I \rangle - \frac{\alpha}{N^2} \langle n_S \rangle \langle n_I \rangle^2, \quad (32)$$

$$\frac{\partial \langle n_I \rangle}{\partial t} = -\gamma \langle n_I \rangle + \frac{\beta}{N} \langle n_S \rangle \langle n_I \rangle + \frac{\alpha}{N^2} \langle n_S \rangle \langle n_I \rangle^2. \quad (33)$$

Here, we the total population is conserved, i.e. $N = n_S + n_I$. Therefore, by focusing on the number of susceptible individuals, we define the constraints $C = N$ and

$$q_I = Q(q_S, x_S, x_I, N) = N - x_I q_I. \quad (34)$$

After applying the Cole-Hopf transformation the reduced DPH reads

$$\mathcal{H}^* = (1 - e^\theta)(N - \eta) \left(\frac{\alpha}{N^2} \eta e^{-\theta} (N - \eta) + \frac{\beta}{N} \eta e^{-\theta} + \gamma \right), \quad (35)$$

where $\eta = \langle n_S \rangle$. The zero-energy lines are given by

$$\begin{aligned} \theta &= 0, & \eta &= N, \\ \Theta(\eta, \beta, \gamma, \alpha) &= \log \left(-\frac{\eta(\eta\alpha - N(\alpha + \beta))}{N^2\gamma} \right). \end{aligned} \quad (36)$$

Within the mean-field approximation, we consider only the fixed points $F = (\eta, \theta)$ with $\theta = 0$, that is,

$$\begin{aligned} F_1 &= (N, 0), \\ F_\pm &= \left(N \frac{\alpha + \beta \pm \sqrt{\alpha^2 + 2\alpha\beta - 4\alpha\gamma + \beta^2}}{2\alpha}, 0 \right). \end{aligned}$$

By solving the system of Eq. (19) and imposing $\alpha, \beta, \gamma \geq 0$, we find two different critical conditions,

$$\beta = \gamma, \quad \beta = -\alpha + 2\sqrt{\alpha\gamma}, \quad (37)$$

and we thus expect to find two distinct phase transitions. We can distinguish these two critical behaviors, as shown in Fig. 1, where one transition occurs for $\alpha < \gamma$ and another for $\alpha > \gamma$. First, we note that the condition $\beta = \gamma$ is a critical point for any α . Indeed, as can be seen in Figs. 1a and 1d, for $\gamma > \beta$, F_1 is the only attractor of the systems (provided that $\langle n_S \rangle \leq N$). When $\beta = \gamma$, the attractor changes. This can also be observed when considering a deterministic approach by means of linearizing the mean-field equations about the fixed point. When doing so, the dynamics around F_1 when $\theta = 0$ reads,

$$\partial_t \eta = (\eta - N) \left(\partial_{\eta, \theta}^2 \mathcal{H}^* \right) \Big|_{F_1} = (\beta - \gamma)(\eta - N). \quad (38)$$

Hence, the asymptotic state varies at $\beta = \gamma$. To fully characterize the critical behavior, the remaining critical condition (Eq. (37)) needs to be studied as well. We note that, at $\beta \geq -\alpha + 2\sqrt{\alpha\gamma}$, two new fixed points F_\pm appear, suggesting the presence of an abrupt transition. When $\beta = -\alpha + 2\sqrt{\alpha\gamma}$, a non-trivial zero-energy line intersects tangentially the mean-field manifold $\theta = 0$ at $F_+ = F_-$. For $\gamma > \alpha$ the tangent point is above the absorbing state F_1 , otherwise it stays below it. Fixing α and γ , with $\gamma > \alpha$, and varying β , we observe that $F_- = F_1$ at $\beta = \gamma$ (Fig. 1b). By further increasing β , the intersection F_- smoothly moves below the absorbing state becoming the new asymptotic state (Fig. 1c), resulting in a second-order phase transition. On the other hand, for $\gamma < \alpha$ we have $F_+ = F_1$ at the critical condition (Fig. 1e), and, for $\beta > \gamma$, F_+ is above the absorbing state (Fig. 1f). In this case, F_- becomes attractive, so the dynamics jumps to F_- and the transition is of first-order.

To summarize, our system is characterized by the fol-

lowing critical behavior:

$$\begin{aligned} \beta &= \gamma && \text{critical condition,} \\ \beta &= \alpha = \gamma && \text{tricritical point,} \\ \alpha &> \gamma && \text{first-order phase transition,} \\ \alpha &< \gamma && \text{second-order phase transition.} \end{aligned}$$

This analysis exemplifies how one should approach the study of critical behavior of CRNs within the context of the Doi-Peliti formalism.

D. The role of the initial conditions

In general, CRNs can exhibit highly non-trivial phase diagrams with many different attractors — especially when the number of compartments grows. Under certain conditions, this may impact the procedure introduced in this work. Indeed, this methodology does not provide the critical point certainly, but indicates conditions in which variations of the topology of the phase space lead to possible changes in the asymptotic dynamical behaviour of the system. Since we are analysing systems that are out of equilibrium, the steady states can depend on the initial conditions, and the dynamical evolution of the system may be independent of the topological configuration variations identified by the formalism. In these cases, the possible phase transitions depend on the initial state and, in general, it is impossible to identify an analytical condition which provides the critical point and characterizes the phase transition.

To illustrate this point, let us consider again the modified *SIS* model, but now with $\beta = 0$. This leaves only the three-body interaction as the sole infection mechanism. By repeating the analysis, we find for this configuration three fixed points along the mean-field line, which are

$$F_1 = (N, 0), \quad F_{\pm} = \left(N \left(\frac{1}{2} \pm \sqrt{\frac{\alpha - 4\gamma}{4\alpha}} \right), 0 \right).$$

After rescaling, i.e. $N = 1$, and solving Eq. (19), the critical condition reads

$$F_- = F_+ = \left(\frac{1}{2}, 0 \right), \quad \alpha = 4\gamma \quad (39)$$

At this condition, new fixed points appear (Fig. 2). According to our expectations, there is a possible first-order transition. However, when assuming $n_S \approx 1$, a phase transition is not observed when numerically integrating the dynamical system. When varying the rates, we can determine the attractive or repulsive character of the fixed points. For $\alpha < 4\gamma$, F_1 is the only attractor (Fig. 2a). For $\alpha > 4\gamma$, if $n_S(0)$ is greater than the fixed value $\frac{1}{2}$, the attractor does not vary, and we can conclude there is no phase transition. In fact, this occurs only when there is an overlap between a hyperbolic fixed point and the initial configuration of the system as shown

in Figs. 2c and 2d. This condition is given by a rate $\tilde{\alpha}$ that can be found by solving $F_+ = (n_S(0), 0)$,

$$\tilde{\alpha}(n_S(0)) = \frac{\gamma}{(1 - n_S(0))n_S(0)}. \quad (40)$$

In the case $n_S(0) \approx 1$, we have $\tilde{\alpha} \rightarrow \infty$, so the system does not display an effective phase transition. On the other hand, if $n_S(0) < \frac{1}{2}$, then the variation of the eigenspace does affect the system and we have an effective phase transition described by the condition of Eq. (39). The existence of this phase transition can be verified by numerical integration for different initial conditions (Fig. 2e).

The very same arguments can be extended to the case with several compartments. However, the solution becomes more complicated because the inherent difficulty to systematically identify which eigenspace a generic initial configuration belongs to. In this case, an alternative solution might be to employ numerical investigations to verify whether the phase transition takes place or not. We, however, provide yet another alternative approach that is related to reducing the dimensions of the system, which we shall now expand on.

IV. DIMENSION REDUCTION

A. Theoretical results

Dynamical models with many components are common and their characterization as Hamiltonian systems can be complicated. Moreover, only in the case of single-compartment systems we are able to find a graphical visualization of the level sets with the tools presented so far. To find a strategy to extend the Doi-Peliti representation to multi-compartment models, we start by noting that the presence of first integrals helps simplify the system. We employ this property to build our own dimension reduction method, which is based on using the deterministic equations as first integrals to freeze the degrees of freedom that are not inherent in the order parameter. From this, we are able to obtain an effective Hamiltonian \mathcal{H}^* that captures the fundamental features of the system.

Let us consider a general DPH for a chemical reaction process. Take the deterministic trajectories

$$\begin{aligned} \partial_t \langle n_1 \rangle &= f_1(\langle n_1 \rangle, \langle n_2 \rangle, \dots), \\ \partial_t \langle n_2 \rangle &= f_2(\langle n_1 \rangle, \langle n_2 \rangle, \dots), \\ &\vdots \\ \partial_t \langle n_d \rangle &= f_M(\langle n_1 \rangle, \langle n_2 \rangle, \dots), \end{aligned} \quad (41)$$

where f_i are functions of occupation numbers obtained by the solutions of the Hamiltonian problem setting $x_j = 1$ and $q_j = \langle n_j \rangle$. Since we are assuming that an asymptotically steady state is reached when $t \rightarrow \infty$, this set of equations admits a solution for $\partial_t \langle n_j \rangle = 0$ for all j . As before, we take I_1 as the starting compartment with

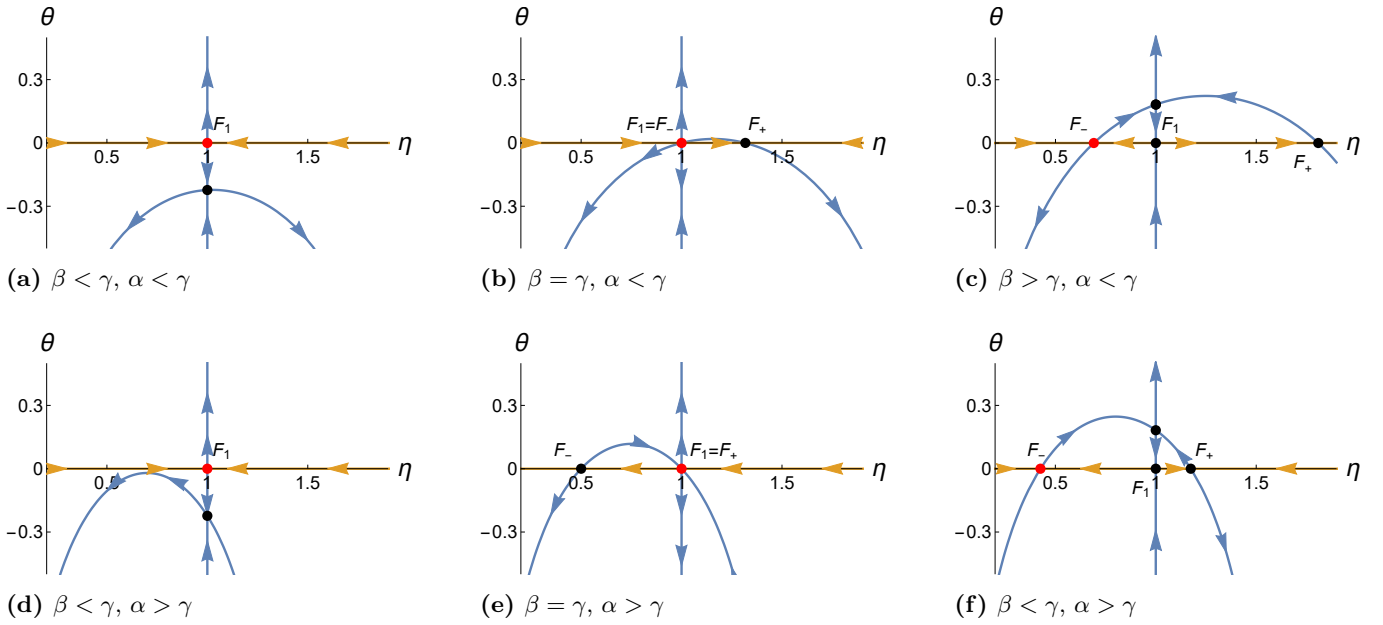


Fig. 1: Phase portrait for the modified *SIS* model by using the Cole-Hopf variables. The orange lines represent the mean-field manifold, while the blue ones are the other non zero-energy lines. The fixed points are F_1 and F_{\pm} . Red dots are the attractors of the deterministic dynamics. In Panels 1a,1c and 1b we show a second-order phase transition: at the critical condition $\beta = \gamma$, F_{-} overlaps with F_1 becoming the new attractor. In the lower Panels 1d,1e and 1f, the first-order transition is reported: at $\beta = \gamma$, $F_1 = F_{+}$ and the attractor changes abruptly.

$\langle n_1 \rangle \approx N$ at $t = 0$. For large t , we rewrite the previous system as

$$\begin{aligned} \partial_t \langle n_1 \rangle &= f_1(\langle n_1 \rangle, \langle n_2 \rangle, \dots), \\ \partial_t \langle n_j \rangle &= 0, \end{aligned} \quad (42)$$

meaning that $f_i(\langle n_1 \rangle, \langle n_2 \rangle, \dots) = 0$ for all $j > 1$ — i.e. for all compartments but the first. In doing so, we are imposing constraints on the average values of the occupation numbers, from which we derive the set of first integrals. Fixing these constraints is equivalent to seeing how all degrees of freedom converge at equilibrium points as a function of a single compartment. We emphasise that the constraints of Eq. (42) regards only the average values of the mean-field approximation. Making an analogy with statistical mechanics, we are setting a constraint on the expectation value of a quantity, similarly to the canonical ensemble constraining the average value of the system energy. Therefore, the physical interpretation of this dimension reduction is as follows: In the large time limit, the averages of occupation numbers converge to a hyperbolic fixed point in an M -dimensional space following the constraints imposed by Eqs. (42).

Further physical insights can be gained by studying what occurs near this limit. Let x_1 and q_1 be the only variables related to the order parameter, while all the other degrees of freedom are frozen. From an analytic point of view, by using Eqs. (42) we can rewrite q_j for all $j > 1$ as functions of q_1 and x_1 . While this is not always possible, we show that we can add a suitable transition

rate to have the Eqs. (42) be solvable without altering the critical environment (see Appendix E). In other words, we can define a parametrization Λ such that

$$\Lambda(x_1, q_1) = \{x_1, x_{\setminus 1} = 1, q_1, q_{\setminus 1} = Q_{\setminus 1}(x_1, q_1)\}, \quad (43)$$

where $x_{\setminus 1} = 1$ denotes that for all $j > 1$ we have $x_j = 1$, and similar for $q_{\setminus 1}$ we have $q_j = Q_j(x_1, q_1)$ with Q_j as defined in Eq. (18). Applying this parametrization to the DPH, we obtain an effective Hamiltonian $\mathcal{H}^* = \mathcal{H} \circ \Lambda$ that only depends on x_1 and q_1 . However, note that the solutions of Eq. (42) can yield different parametrizations. These may represent different states of the system, where the corresponding reduced Hamiltonians have different hyperbolic fixed points. To take the correct \mathcal{H}^* , we can investigate the stability of the fixed points of the full problem, and choose the parametrization such that \mathcal{H}^* has the same attractor as the complete system.

To be more specific, we define a domain of Λ in the parameter space. The points at which two different parametrizations provide the same reduced dynamics are generally critical points (see also Appendix F 4). Moreover, for many systems the conservation of the total population number hold, hence reducing the dimension of the problem by one. So, by applying the reduction procedure, we substitute one mean-field equation by Eq. (34). As before, we have an extra degree of freedom since we can derive different Λ depending on the first integrals that we are choosing. However, that does not change the deterministic description. In fact, despite the multiplicity of Hamiltonians \mathcal{H}^* , if the corresponding Λ satisfies

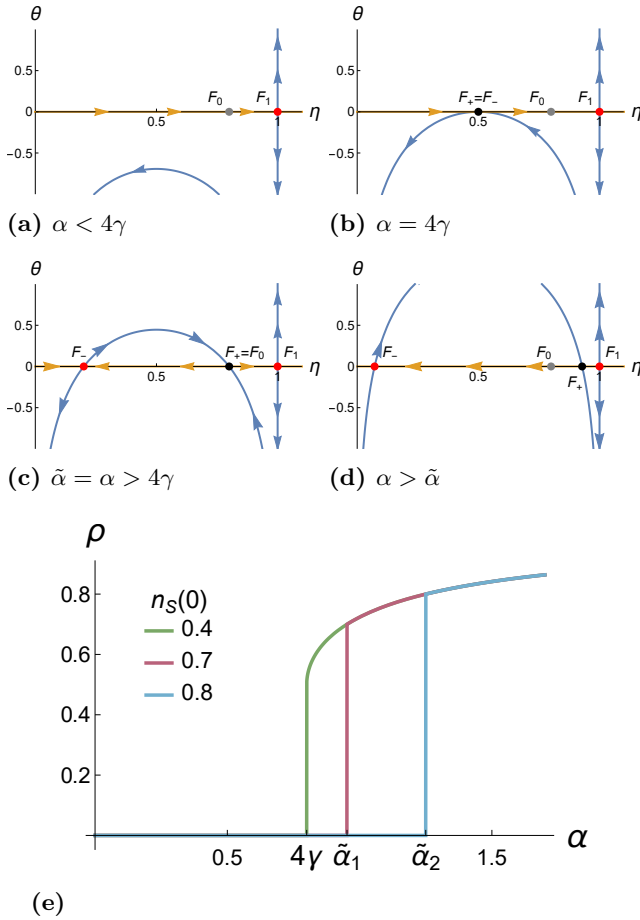


Fig. 2: Characterization of the critical behavior of the two-compartment system with a three-body interaction (modified *SIS* model of Sec. III C). From panels (a) to (d), the orange lines represent the mean-field manifold, while the blue one are the other zero-energy lines. Red dots are the attractors of the deterministic dynamics. F_0 represent the initial condition. In (e), we display the order parameter as a function of the parameter controlling the strength three-body interaction, obtained from simulations. For the numerical experiments, we have considered $\gamma = 0.2$ and we have normalized the population setting $N = 1$. We observe that for $n_S(0) > 1/2$ the phase transition occurs for $\alpha > 4\gamma$. Here $\tilde{\alpha}_1 = 0.953$ and $\tilde{\alpha}_2 = 1.25$ as predicted by Eq. (40). Moreover, for all initial conditions, the active phase is described by the same curve: this curve is given by the value of F_- as a function of α .

the condition discussed above, the fixed points and the asymptotic behaviour of the system do not vary. Otherwise, from a stochastic point of view, we have different Langevin equations (see Eq. (25)).

Our approach binds the system by imposing certain degrees of freedom fixed in their steady state. This means that the stochastic information that we get is related to the conditional probability $p(n_1|n_2, \dots, n_{N-M})$, which we

are taking as an approximation for $p(n_1)$ in the stationary limit. Different parametrizations lead to different constraints, and thus to different conditional probabilities. In this case we can write several Langevin equations that will be only qualitative estimates of the stochastic properties of the system, such as the stationary probability distribution. In Appendix F 2 we discuss an example in more detail.

As a final remark on the parametrization Λ , we note that it is associated to the (x, q) -coordinates. Indeed, it is defined from the mean-field trajectories that are functions of the variables q only. If we were to use the Cole-Hopf variables of Eq. (D3) instead, we would get a transformation in terms of η , which is linked to the previous coordinates by $\eta_j = x_j q_j$. Considering that we are imposing $x_j = 1$ for $j > 1$, the two representations are equivalent only if we substitute $\langle n_1 \rangle$ in Eq. (13) with $x_1 q_1$ instead of q_1 . This would, however, be incorrect, as we would go beyond the mean-field approximation and additionally constrain fluctuations. Therefore, we must define Λ by using the (x, q) -coordinates, and only after doing this we can apply the Cole-Hopf transformation and obtain a physical interpretation of the fields. We want to emphasize that, while the reduction holds only at the large time limit, it remains useful for the study of the system near the critical condition. Similar to the work in Ref. [25], our goal is to create an analogy with Landau theory, which, in equilibrium statistical mechanics, offers a way to analyse the critical behaviour of a system [47]. Defining the effective Landau free energy \mathcal{L} , one can study the phase transitions by finding the minima of \mathcal{L} . By employing the Doi-Peliti formalism, we can extend this approach for non-equilibrium systems, by introducing \mathcal{L} by \mathcal{H}^* and, instead of observing the minima of the former, focusing on the fixed points of the latter instead.

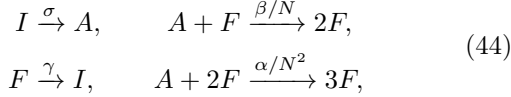
We would like to note that our formalism does not pretend to give an exact characterization of the system's stochastic behavior. Instead, our approach qualitatively describes this with an effective Langevin equation that we obtain within a single framework. Within this framework, we derive both the deterministic limit and investigate critical points. In the absence of this ambiguity, our dimension reduction scheme proves to be a useful way to describe the stochastic behavior of a variety of models, which will now be applied to study CRNs in the remainder of this paper.

Before this, we would like to mention that deterministic studies of the critical behaviour, such as the one we propose in Eq. (19), can additionally be done with other approaches. For example, by obtaining a one-dimensional effective mean-field equation using our method, we can define an effective potential, as is done in Ref. [48], and investigate the phase transition by studying its minima. However, our approach offers an alternative to geometrically attack a broad class of problems. It does not only allow us to go beyond the mean-field description, but also allows for using path-integral representations to

complex physics problems.

B. Application to cascading failures: A modified SIRS model

Let us begin displaying the strength of our proposed framework by considering a modified version of the SIRS model, which now, in contrast with the previously analysed SIS model, contains an additional compartment [49]. We assume that the three compartments correspond to active, A , damaged (failed), F , or inactive, I , states. The elementary reactions read



where σ is the recovery rate of failed units, γ the transition rate of failed units to inactive ones, and α and β denote the ‘‘infection’’ reaction rates corresponding to three-body long-range failures related to cascading failures, and the standard failure belonging to local spread of failures. Hence, the model differs from a standard SIRS-model as we include a three-body interaction¹ with rate α/N^2 . This reaction can be interpreted as the effect of a field mediating the higher-order effect and is the all-to-all (fully-connected) limit of a model that, when studied in infrastructural or social interconnected systems, is used to describe the non-local unfolding of cascading failures. These cascading effects are observed, for instance, in electrical power grids [50] or in communication networks [51].

We apply on this model the methodological pipeline defined above. The Doi-Peliti Hamiltonian reads

$$\begin{aligned} \mathcal{H} = & \frac{\beta}{N} a_F^\dagger (a_F^\dagger - a_A^\dagger) a_F a_A \\ & + \frac{\alpha}{N^2} (a_F^\dagger)^2 (a_F^\dagger - a_A^\dagger) a_F^2 a_A \\ & + \gamma (a_I^\dagger - a_F^\dagger) a_F + \sigma (a_A^\dagger - a_I^\dagger) a_I, \end{aligned} \quad (45)$$

and the mean-field equations are given by

$$\partial_t \langle n_A \rangle = -\frac{\beta}{N} \langle n_A \rangle \langle n_F \rangle - \frac{\alpha}{N^2} \langle n_A \rangle \langle n_F \rangle^2 + \sigma \langle n_I \rangle, \quad (46)$$

$$\partial_t \langle n_F \rangle = \frac{\beta}{N} \langle n_A \rangle \langle n_F \rangle + \frac{\alpha}{N^2} \langle n_A \rangle \langle n_F \rangle^2 - \gamma \langle n_F \rangle, \quad (47)$$

$$\partial_t \langle n_R \rangle = \gamma \langle n_F \rangle - \sigma \langle n_I \rangle. \quad (48)$$

As done before, we set $\partial_t \langle n_R \rangle = 0$, and by including also the conservation of total population N , which we re-scale to $N = 1$, we obtain the transformations

$$q_F = \frac{1 - x_A q_A}{\gamma + \sigma}, \quad q_R = \frac{1 - x_A q_A}{\gamma + \sigma} \gamma.$$

The Cole-Hopf Hamiltonian related to the reduced problem is

$$\begin{aligned} \mathcal{H}^* = & -(\gamma + \sigma)^{-2} \left\{ (\eta - 1) e^{-\theta} (e^\theta - 1) \sigma [\alpha(\eta - 1) \eta \sigma \right. \\ & \left. - \beta \eta (\gamma + \sigma) + \gamma e^\theta (\gamma + \sigma)] \right\}, \end{aligned} \quad (49)$$

and the zero-energy lines are

$$\eta = 1, \quad \theta = 0,$$

and

$$\begin{aligned} \theta = & \Theta(\eta, \beta, \gamma, \alpha, \sigma) \\ = & \log \left(-\frac{\eta(\alpha\eta\sigma - \alpha\sigma - \beta\gamma - \beta\sigma)}{\gamma(\gamma + \sigma)} \right). \end{aligned}$$

These curves show the same structure as the ones of the modified SIS model (see Section IV B), thus we recover the same topology reported in Fig. 1, and the same phase portraits shown in Fig. A3. Therefore, we have three fixed points on $\theta = 0$: $F_1 = (1, 0)$ and F_\pm . We expect to $\gamma = \beta$ to be a critical point, whose nature is conditioned by the three-body interaction mediated by α . For α larger than a certain threshold $\tilde{\alpha}$, the system will display a first-order, abrupt transition, while otherwise a second-order appears. By studying Θ , we note that the sign of the eigenvalues along the mean-field manifold changes at $\beta = \gamma$ since $\Theta(\eta, \beta, \beta, \alpha, \sigma) = 0$. In the range $\beta > \gamma$, the fixed points F_\pm become the new attractors. Let us focus now on the attractor with $\eta \leq 1$. If at $\beta = \gamma$ we have $F_+ = F_1$, then the new attractor in the active phase is F_- , and so there is an abrupt transition. Again, this happens when $\alpha > \tilde{\alpha}$. When $\alpha < \tilde{\alpha}$, at the critical point we have $F_- = F_1$, and the new attractor at $\beta > \gamma$ is still F_- . In this case, the position of the attractor varies smoothly, and so there is a second-order phase transition.

Further insights on the critical behavior can be obtained by investigation of Θ . Indeed, the tricritical condition, i.e., $\gamma = \beta$ and $\alpha = \tilde{\alpha}$ such that $F_1 = F_\pm$, corresponds to the solution of the following system

$$\begin{aligned} \Theta(\eta, \beta, \gamma, \alpha, \sigma) = \frac{\partial}{\partial \eta} \Theta(\eta, \beta, \gamma, \alpha, \sigma) = 0, \\ \eta = 1, \\ \beta = \gamma \end{aligned}$$

We find that the tricritical point in the parameter space is given by

$$\begin{aligned} \beta = \gamma, \\ \tilde{\alpha} = \gamma(\gamma + \sigma)/\sigma. \end{aligned} \quad (50)$$

These results are consistent with the deterministic description of the system. Furthermore, following the strategy discussed in Section III B, we can investigate the behavior beyond the mean-field limit. For this purpose, we analyse the statistical fluctuations of the state of the system. Using the expression of Eq. (49) for the reduced Hamiltonian \mathcal{H}^* , the reduced Langevin equation of Eq. (25) reads

$$\frac{d\eta}{dt} = \left(\frac{\sigma(N - \eta) (\gamma N^2(\gamma + \sigma) - N\eta(\alpha\sigma + \beta(\gamma + \sigma)) + \alpha\sigma\eta^2)}{N^2(\gamma + \sigma)^2} \right) + \left(\frac{\sigma(N - \eta) (\gamma N^2(\gamma + \sigma) + N\eta(\alpha\sigma + \beta(\gamma + \sigma)) - \alpha\sigma\eta^2)}{N^2(\gamma + \sigma)^2} \right)^{\frac{1}{2}} \cdot \xi. \quad (51)$$

We compare between the order parameter for the reduced dynamics and for the full dynamics carried out by the Kramers-Moyal expansion, and illustrate this comparison in Fig. 3. We observe that, for t large, the reduced mean-field dynamics converges to the complete one, and the fluctuations display similar statistical properties in both cases. Indeed, in Fig. 3 we give a comparison between the stationary probability distribution function (PDF) of the full system and the one derived from the reduced dynamics. In the case of reduced dynamics, its PDF is given by Eq. (26). These figures indicate a good agreement between our approximations and the real distribution, displaying the efficacy of our approach.

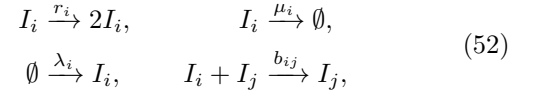
This example highlights that we can analyse the critical environment of a system by studying a simple function Θ . This demonstrates one of the advantages of our approach. Given a multidimensional system of which we want to characterize some of its critical features, we can systematically follow the steps of our formalism to reduce all the complexity to an analysis of some parametric functions. That said, our approach is not limited to providing insights into the critical properties, but also offers quantitative assessments on the properties of the steady state, such as the value of the order parameter and its distribution. In the next sections, we shall provide a more detailed explanation of this.

C. Application to ecology: the generalized Lotka-Volterra model

Let us now turn our attention to ecological systems. Within this context, one most often considers the generalized Lotka-Volterra model, which describes the dynamics of many interacting species. Recently, this model has been used to investigate biodiversity, with the aim of providing an answer to the so-called ‘diversity-stability’-paradox, as theoretical approaches indicate that diversity should hamper stability [52–54], yet observational studies find the exact opposite must be true [55]. More recently, dynamical mean-field theory has been applied to the generalized Lotka-Volterra model with great success [56, 57], and there have been successful attempts at

describing the Lotka-Volterra model as a chemical reaction network [27]. Yet, to the best of our knowledge, reduced dynamics (stochastic) Lotka-Volterra models have not been put forward, but yet may provide valuable insights in (critical) behavior of complex ecological models.

To this end, let us study the stochastic Lotka-Volterra model. This model can be described by the following elementary reactions for each of the species I_i ,

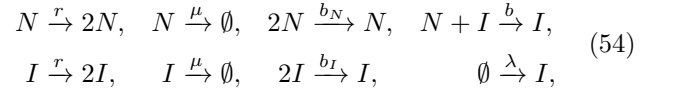


where r_i , μ_i and λ_i are, respectively, the growth, death and migration rate of species i , and b_{ij} is the interaction coefficient that captures the effect of species j on species i (see, e.g., Ref. [27], for more details). The DPH of the Lotka-Volterra model reads

$$\begin{aligned} \mathcal{H} = & \sum_i r_i a_i^\dagger (a_i^\dagger - 1) a_i + \sum_i \lambda_i (a_i^\dagger - 1) \\ & + \sum_i \mu_i (1 - a_i^\dagger) a_i + \sum_{i,j} b_{ij} a_i^\dagger (1 - a_j^\dagger) a_i a_j. \end{aligned} \quad (53)$$

1. A simple two-species Lotka-Volterra system

As an example, we consider a simple two-species system consisting of native and invasive species, denoted with N and I , that compete. The elementary reactions for this example read



where b_I and b_N are the self-regulation term corresponding to an effective carrying capacity, b is the effect of the invasive species on the native one, and λ is the migration rate (invasion rate) of the invasive species. In this case, the DPH reads

$$\begin{aligned} \mathcal{H} = & r \left(a_I^\dagger (a_I^\dagger - 1) a_I + a_I^\dagger (a_I^\dagger - 1) a_I \right) + \lambda (a_I^\dagger - 1) \\ & + \mu \left((1 - a_I^\dagger) a_I + (1 - a_N^\dagger) a_N \right) \\ & + b a_I^\dagger (1 - a_N^\dagger) a_N a_I \\ & + b_I a_I^\dagger (1 - a_I^\dagger) a_I^2 + b_N a_N^\dagger (1 - a_N^\dagger) a_N^2 \end{aligned} \quad (55)$$

¹ Note that this is similar to the three-body interaction we introduced in the modified *SIS*-model that was discussed in Section IV B.

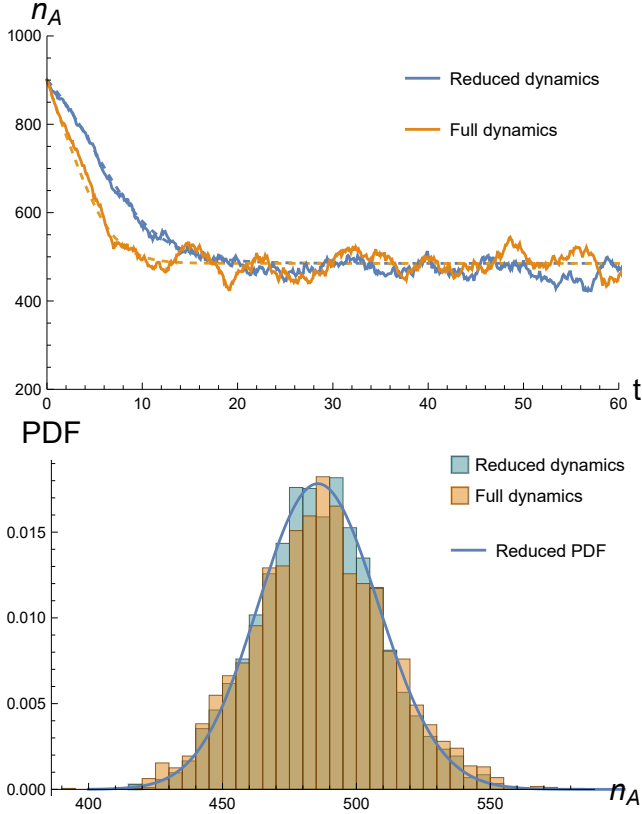


Fig. 3: Top: Numerical simulation for the modified *SIRS* model. We have considered $N = 10^3$, $\beta = 0.8$, $\gamma = 0.4$, $\alpha = 0.15$ and $\sigma = 1$. The dashed lines represent the deterministic dynamics for both the reduced and the full system. The solid lines are the stochastic trajectories generated by Eq. (25) applied to \mathcal{H} and to \mathcal{H}^* . Bottom: Probability distribution function at the stationary limit of the modified *SIRS* model. The blue histogram represents the PDF obtained by the long time behaviour of numerical simulations realized considering the reduced dynamics. The orange one is the distribution related to the full system. The solid blue line depicts the analytic reduced PDF given by Eq. (26). Relevant parameters are $N = 10^3$, $\beta = 0.8$, $\gamma = 0.4$, $\alpha = 0.15$ and $\sigma = 1$.

In order to proceed, we consider $b_N, b_I, b \ll 1$ to work in the range of validity of our theory, i.e., the chemical reaction follow the scaling rule of Sec. II C. Moreover, we assume that $b_I > b$, that is, the carrying capacity of the invasive species is not so large to dominate the native species for any migration rate $\lambda > 0$. We choose the asymptotic population of the native species N as the order parameter and derive the reduced Hamiltonian using Eq. (42). We solve the system using the invasion rate λ as a free parameter, and we obtain a critical value

$$\tilde{\lambda} := \frac{(r - \mu)^2(b_I - b)}{b^2}. \quad (56)$$

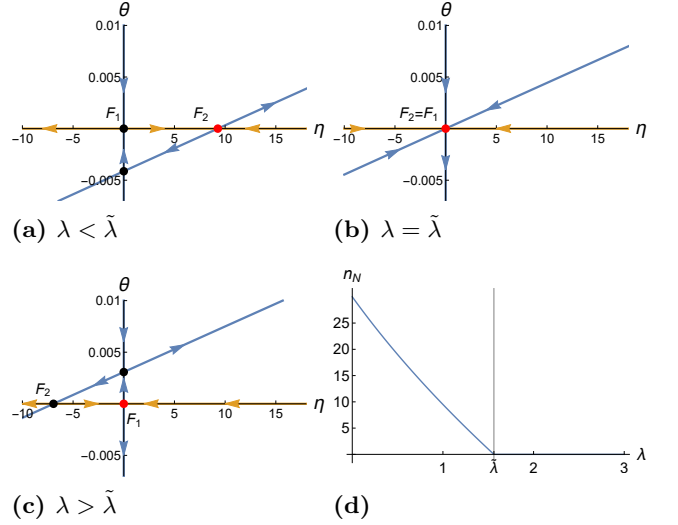


Fig. 4: Reduced dynamics of the Lotka-Volterra model. For $\lambda < \tilde{\lambda}$ the attractor is F_2 with $n_N > 0$. At the critical condition we have the superposition of the fixed points $F_1 = F_2$, and the native species goes to the extinction for larger λ . As confirmed by the numerical integration in Fig. (4d), this is a second order phase transition. We have considered $b = 0.75$, $b = 0.7$, $r = 1/2500$, $r_A = 1/2000$ and $r_B = 1/3000$. With these values we have $\tilde{\lambda} = 1.563$.

The critical points for the reduced model are

$$F_1 = (0, 0),$$

$$F_2 = \left(\frac{r - \mu}{b_N} - \frac{b \left(\sqrt{(r - \mu)^2 + 4b_I \lambda} - \mu + r \right)}{2b_I b_N}, 0 \right).$$

For $\lambda > \tilde{\lambda}$ the native species is driven to extinction by the invasive one (Panel 4c), and $n_B \rightarrow 0$ for $t \rightarrow \infty$. When $\lambda < \tilde{\lambda}$ we find that the two species can coexist (that is $n_N > 0$) as shown in Panel 4a. For lower effective growth rates $r - \mu$, asymptotic abundances of the native species reduce, indicating that slow growing species are more sensitive to invasion. By careful investigation of the phase portrait (Fig. 4), it becomes clear that at the critical point $\lambda = \tilde{\lambda}$ the two fixed points overlap and the native species is driven to extinction (see Fig. 4b). As the equilibrium state changes smoothly, the extinction phase transition is of second order. We report a numerical simulation in Fig. 4d.

2. The Lotka-Volterra system with 8 species

Consider now a stochastic Lotka-Volterra model with a larger number of species to illustrate how the dimension reduction can provide a very good approximation for the asymptotic distributions. We take an 8-species I_i model governed by the reactions of Eq. (52). We let

$r_i = \lambda_i = 1/2$ and $\mu_i = 0$, and specify the interaction matrix \mathbf{B} , with elements b_{ij} , as

$$\mathbf{B} = \frac{1}{1000} \begin{pmatrix} 1 & 1 & \frac{1}{2} & 0 & \frac{3}{10} & 0 & 0 & 0 \\ \frac{1}{15} & \frac{11}{10} & 0 & 0 & \frac{1}{17} & 0 & 0 & 0 \\ 0 & 0 & \frac{4}{5} & 0 & 0 & 1 & 0 & 0 \\ 0 & 0 & 0 & 1 & 0 & 0 & 0 & \frac{1}{9} \\ 0 & 0 & 0 & 0 & \frac{11}{10} & 0 & 0 & 0 \\ 1 & 0 & 0 & 0 & 0 & 1 & 0 & 0 \\ 0 & 0 & 0 & 0 & 0 & 0 & \frac{9}{10} & 0 \\ \frac{1}{6} & 0 & 0 & 0 & 0 & 0 & \frac{1}{5} & 1 \end{pmatrix}. \quad (57)$$

While we do not explore possible phase transitions here (for that, see [54, 56], among others), we will focus here on an analysis of the reduced Langevin dynamics instead. The DPH for this system is given by Eq. (53). Without loss of generality, we will use the first species as the order parameter. A Langevin equation as in Eq. (25) can then be obtained, for which the stationary distribution of the focal species can be derived by numerical integration (Fig. 5). The results of our reduction procedure are in excellent agreement with numerical integration of the full system, highlighting again the strength of our proposed method.

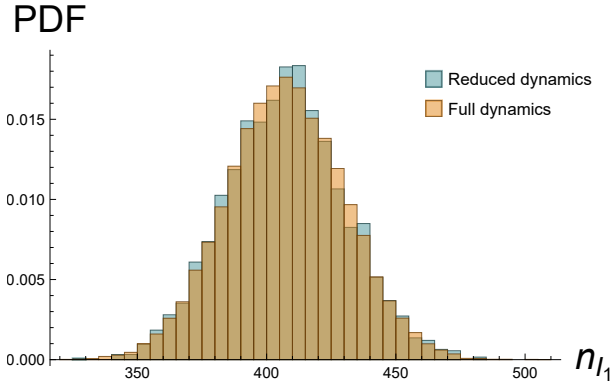


Fig. 5: Numerical asymptotic abundance distribution of the species I_1 of a system described by the generalized Lotka-Volterra model with 8 species. Orange bars represent the normalized probability distribution obtained by numerical integration of the one-dimensional reduced system, while blue bars are results from numerical integration of the full system. We have considered $r = \lambda = 1/2$ and \mathbf{B} given by Eq. (57).

D. Resource-exploiter model

In this last section we treat an ecological model which describes the interactions between resources R , exploiters E and pollutants X . The rationale behind this model is that there are resources that can be used and transformed into something else (e.g., goods, infrastructure, etc.) because of interactions with a population of exploiters. The process of transformation of resources comes at some

cost: it produces pollutants that in part can be re-used to produce other resources. A typical example of the last process is the production of CO_2 due to human activities and the partial re-absorption of this gas by plants to produce new resources (e.g., oxygen, plant-matter that feeds herbivores, agricultural uses, etc.).

By denoting with n_R , n_E and n_X the corresponding occupation numbers, we can model such a system by assuming the following transition rates:

$$\begin{aligned} \omega(\mathbf{n} + \mathbb{I}_R | \mathbf{n}) &= \alpha n_R, \\ \omega(\mathbf{n} + \mathbb{I}_E, \mathbf{n}) &= \mu n_E, \\ \omega(\mathbf{n} - \mathbb{I}_R | \mathbf{n}) &= n_X \xi + \frac{\alpha}{k_R} n_R (n_R - 1), \\ \omega(\mathbf{n} - \mathbb{I}_E | \mathbf{n}) &= n_E \delta + \frac{\mu}{k_E} n_E (n_E - 1), \\ \omega(\mathbf{n} - \mathbb{I}_E + \mathbb{I}_X | \mathbf{n}) &= \beta n_E n_R, \\ \omega(\mathbf{n} + \mathbb{I}_R - \mathbb{I}_X | \mathbf{n}) &= \beta \sigma n_R n_E + \psi n_X n_R, \\ \omega(\mathbf{n} + \mathbb{I}_E - \mathbb{I}_X | \mathbf{n}) &= \beta \gamma n_E n_R. \end{aligned}$$

To reflect the constraints of empirical systems, we are considering a case with resources limited by the capacity k_R . Exploiters consume resources to their advantage while producing pollutants and this interaction is here represented by a contact process: accordingly, the rate is proportional to $n_E n_R$. By exploiting the resources R , E increases, yet their abundance is also limited a carrying capacity k_E . The carrying capacities prevent unbounded population growth. Exploiters are further subjected to natural birth and death processes with rates μ and δ respectively. Resources grow with rate α (e.g., this generation can be due to the injection of energy into the system, such as the one reaching the Earth which is due to the sun) and can be recovered from X by means of two contact interactions: $\beta \sigma n_E n_R$, thanks to the exploiters, and $\psi n_X n_R$. Finally, the pollutants reduce the number of resources by means of the rate ξ .

We note that this system is hard to analyse using available tools, such as the next-generation matrix. The reason is that the pollutants X , which one might interpret as the “infected” counterpart as in standard epidemiological models, can be generated by processes that are independent of their abundance (see the system definition, and Eq. (61)). In epidemiological terms, the “disease-free” equilibrium is not stable, as the infected compartment can grow even when its abundance has reached zero. This contradicts the main assumptions underlying the next-generation matrix [15, 58]. By contrast, while our formalism does not provide an interpretation of epidemic-related measures, such as the basic reproduction number, it can be applied to systems where the main assumptions underlying the next-generation matrix do not hold.

We proceed by deriving DPH for this system, which

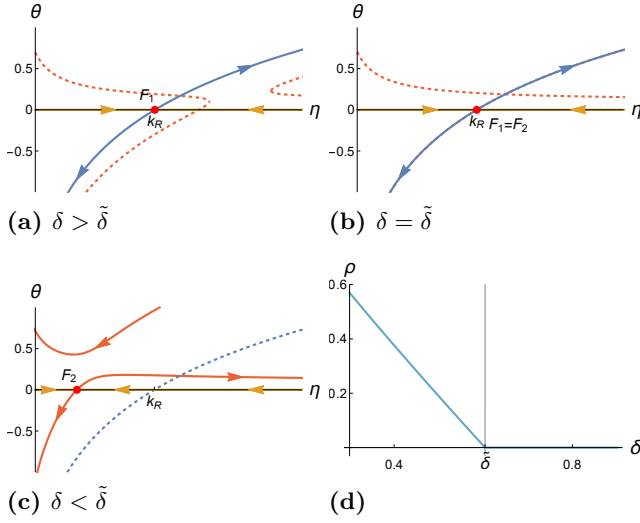


Fig. 6: Phase transition for the resource-exploiter model. Figs. 6a, 6b and 6b show the phase portraits of the reduced system, where the orange line is the mean-field manifold, the blue ones are the zero-energy lines of $\mathcal{H}^{*(A)}$ while the red curves are related to $\mathcal{H}^{*(B)}$. Red dots represent the fixed points on the mean-field manifold. We observe the superposition of the attractors of $\mathcal{H}^{*(A)}$ and $\mathcal{H}^{*(B)}$ at $\delta = \tilde{\delta}$. The solid lines represent the effective phase portrait, while the dashed ones are related to the alternative parameterization that does not represent the system. In Panel. 6d we report a numerical simulation of the model with $\beta = 9 \cdot 10^{-6}$, $\gamma = 8 \cdot 10^{-2}$, $\sigma = 0.1$, $\epsilon = 0.9$, $\psi = 10^{-5}$, $\mu = 0.1$, $\alpha = 0.3$, $k_R = 7 \cdot 10^5$ and $k_E = 8.5 \cdot 10^5$. The critical point is given by $\tilde{\delta} = 0.604$.

reads

$$\begin{aligned}
\mathcal{H} = & \alpha a_R^\dagger (a_R^\dagger - 1) a_R + \mu a_E^\dagger (a_E^\dagger - 1) a_E \\
& + \xi a_X^\dagger a_X \left((a_R^\dagger)^{-1} - 1 \right) + \frac{\alpha}{k_R} a_R^\dagger (1 - a_R^\dagger) a_R^2 \\
& + \frac{\mu}{k_E} a_E^\dagger (1 - a_E^\dagger) a_E^2 + \delta (1 - a_E^\dagger) a_E \\
& + \beta a_E^\dagger (a_X^\dagger - a_R^\dagger) a_R a_E \\
& + \beta \sigma a_R^\dagger (a_R^\dagger (a_X^\dagger)^{-1} - 1) a_R a_E^\dagger a_E \\
& + \psi a_R^\dagger (a_R^\dagger - a_X^\dagger) a_R a_X \\
& + \gamma \beta a_R^\dagger (a_E^\dagger (a_X^\dagger)^{-1} - 1) a_E a_R^\dagger a_R
\end{aligned} \tag{58}$$

Using this expression, we obtain the following mean-field equations:

$$\partial_t \langle n_R \rangle = \alpha \langle n_R \rangle \left(1 - \frac{\langle n_R \rangle}{k_R} \right) - \beta \langle n_E \rangle \langle n_R \rangle - \xi \langle n_X \rangle + \beta \sigma \langle n_R \rangle \langle n_E \rangle + \psi \langle n_R \rangle \langle n_X \rangle \tag{59}$$

$$\partial_t \langle n_E \rangle = \mu \langle n_E \rangle \left(1 - \frac{\langle n_E \rangle}{k_E} \right) + \beta \gamma \langle n_R \rangle \langle n_E \rangle - \delta \langle n_E \rangle \tag{60}$$

$$\partial_t \langle n_X \rangle = (1 - \sigma - \gamma) \beta \langle n_R \rangle \langle n_E \rangle - \psi \langle n_R \rangle \langle n_X \rangle \tag{61}$$

The WKB approximation is valid when the following conditions are satisfied: (1) $k_R, k_E \gg 1$, meaning that we consider relatively large populations and that we are able to apply a system size expansion, and (2) $\beta, \psi \ll 1$, in order to rescale the contact processes with respect to the size of the system. We consider $\rho = 1 - \lim_{t \rightarrow \infty} \langle n_R(t) \rangle / k_R$ as the order parameter. By letting $\partial_t \langle n_E \rangle = \partial_t \langle n_X \rangle = 0$ we obtain two different parametrizations, A and B , that read

$$\Lambda_A = (x_R, x_E = 1, x_X = 1, q_R, q_E = 0, q_X = 0),$$

$$\Lambda_B = (x_R, 1, 1, q_R,$$

$$\frac{k_E}{\mu} (q_R \beta \gamma - \delta + \mu), \frac{k_E \beta}{\mu \psi} (q_R \beta \gamma - \delta + \mu) (1 - \gamma - \sigma)).$$

By solving Eq. (19), we identify $\tilde{\delta} = \mu + \gamma \beta k_R$ as a critical point. By using Λ_A , the Cole-Hopf reduced Hamiltonian reads

$$\mathcal{H}_A^* = \frac{\alpha \eta e^{-\theta} (e^\theta - 1) (e^\theta k_R - \eta)}{k_R}, \tag{62}$$

or, by employing Λ_B instead, we find

$$\mathcal{H}_B^* = \frac{e^{-2\theta}(e^\theta - 1)}{k_R \mu \phi} \left(\eta e^{2\theta} k_R \phi (\alpha \mu + \beta(\gamma - 1) k_E (\delta - \mu)) + \beta^2 \gamma \eta k_R k_E (\epsilon(\gamma + \sigma - 1) - \eta \phi) \right. \\ \left. - e^\theta (\alpha \eta^2 \mu \phi + \beta k_R k_E (\eta \phi (\beta(\gamma - 1) \gamma \eta - \delta + \mu) + \epsilon(\gamma + \sigma - 1)(\delta - \mu))) \right) \quad (63)$$

By studying the eigenvalues of the deterministic system, we find that $\langle n_R \rangle = k_R$ is the attractor for $\delta > \tilde{\delta}$ (Fig. 6a), otherwise the attractor is one of the mean-field fixed point of \mathcal{H}_B^* as reported in Fig. 6c. Following the discussion of Section IV, \mathcal{H}_A^* is well defined for $\delta > \tilde{\delta}$, while \mathcal{H}_B^* represents the system for $\delta < \tilde{\delta}$. The energy levels of both reduced Hamiltonians are shown in Fig. 6. From Figs. 6a to 6c, we note that the attractors exchange their position in a continuous manner at the critical point, which denotes a second-order transition. This is confirmed by numerical simulations (Fig. 6d).

Since the DPH contains many parameters, it is difficult to explore all possible ranges. Indeed, the system exhibits (numerical) instabilities, for example when δ is very small. When Eqs. (59) to (61) converge to an equilibrium point (as is the case in Fig. 6), and thus satisfies the stability condition necessary for our approach, we see instead that we are able to fully characterize the critical behaviour using our method.

V. CONCLUSIONS

In this work we have presented a unifying framework that shows how to systematically apply the Doi-Peliti formalism to a broad class of compartmental models. Several studies have proven how path integral approaches can offer advantages when describing stochastic systems, characterizing phase transitions and giving information beyond the deterministic limit. Yet, dealing with systems with many compartments is generally complicated, especially regarding the visualization of the geometry of phase portraits to identify the nature of the phase transitions. Here we have derived a novel strategy that allows us to unify these descriptions thanks to the introduction of a dimension reduction scheme. In practice, through our method we gain information about the nature of the phase transitions, and analyze both qualitatively and quantitatively the stochastic dynamics. We do so through a transparent physical interpretation: since the observable of interest, the order parameter, corresponds to a single compartment, one can freeze all other degrees of freedom and study only the compartment corresponding to the observable.

We have illustrated the usefulness of this methodology by applying it to several multi-compartmental stochastic processes of increasing complexity and of different nature, including epidemiological, ecological and sociotechnical ones. Starting from the simplest case of two-

compartment systems, we have explored the role that three-body interactions, recently reported to significantly impact the behavior of many empirical systems [59], play on the critical aspects of epidemiological-inspired models. This opens the door to systematically analyze systems whose interactions are beyond pairwise. For systems with more than two components, our dimension reduction proposal offers very good approximations for the stationary probability density function of the order parameter, and successfully captures their critical properties.

To derive our dimension reduction scheme, we have used some approximations that do not impact the predictions of the critical behavior, yet they do have an effect on the transient dynamics. Indeed, many methods of dimensionality reduction aim to describe not only the stationary limit, but also to provide information about the whole dynamics, which is however often at the expense of needing more assumptions. Hence, there is a compromise between the amount of information one can analytically retrieve and the generality of the model one can actually study. Our method positions itself in a place in which it can be generally applied to a range of systems that is wider than what traditional methods, such as those based on time scale separation [60, 61], offer, but it misses the possibility of an accurate prediction of the transient phase.

Offering insights on the transient dynamics from the point of view developed here remains as a future research perspective. Additionally, our method is most useful in scenarios in which only one degree of freedom is effectively operating in the long-time behaviour, so it not yet clear how to reduce the dimensionality in a case with coupled degrees of freedom. Another aspect that we believe is worth further consideration is related to the parametrization Λ and the reduced Hamiltonian, $\mathcal{H}^* = \Lambda \circ \mathcal{H}$. More specifically, the difficulties are associated with the definition of the validity domain and the potential degeneration of Λ . A remaining open question, which we foresee having a great impact due to the wealth of potential applications, is the generalization of this dimension reduction scheme to structured, networked populations [62].

All in all, we have exploited the combination of the path-integral representation of stochastic processes with a dimension reduction scheme to better understand the critical properties and the stationary behavior of coupled compartmental stochastic processes. We hope that our formalism will provide new perspectives and physical insights into, and beyond, the characterization of phase

transitions and fluctuation dynamics multi-compartment complex systems.

ACKNOWLEDGMENTS

O.A. acknowledges financial support from the Spanish Ministry of Universities through the Recovery, Transformation and Resilience Plan funded by the European Union (Next Generation EU) and the University of the Balearic Islands. J.N. acknowledges financial support from the Human Frontier Science Program Organization (HFSP Ref. RGY0064/2022). M.D.D. acknowledges partial financial support from the MUR - PNC (DD n. 1511 30-09-2022) Project no. PNC0000002, DigitAl life-long pRevEntion (DARE); from MUR funding within the PRIN 2022 PNRR (DD n. 1214 31-07-2023) Project no. P2022A889F and from MUR funding within the FIS (DD n. 1219 31-07-2023) Project no. FIS00000158. T.S. acknowledges financial support from the University of Padua (PRD-BIRD 2022).

Appendix A: Derivation of the path integral representation

Here we show the derivation of the path integral representation for the generating function $|G\rangle$ by using the Doi-Peliti formalism as done in [24]. Let us take the simplest one-compartment case $|\mathbf{n}\rangle = |n\rangle$ with the basis (9). We take also \mathcal{H} in its normal ordered form. By writing the time dependency explicitly $|G\rangle = |G(t)\rangle_x$ and by splitting t in infinitesimal intervals $t = M\epsilon$ with $\epsilon \rightarrow 0$ and $M \rightarrow 0$, we have

$$\begin{aligned} |G(t)\rangle_x &= e^{\epsilon\mathcal{H}(a^\dagger, a)} |G(t-\epsilon)\rangle_x + O(\epsilon) \\ &= \int_{\mathbb{R}} dx_{M-1} e^{\epsilon\mathcal{H}(x, \partial_x)} \delta(x - x_{M-1}) |G(t-\epsilon)\rangle_x + (O(\epsilon^2)) \\ &= \int_{\mathbb{R}^2} \frac{dx_{N-1} dq_{N-1}}{2\pi} e^{\epsilon\mathcal{H}(x_N, iq_{N-1})} \\ &\quad \times e^{-iq_{N-1}(x_{N-1} - x_N)} |G(t_{N-1})\rangle_{x_{N-1}} + O(\epsilon^2) \\ &= \int_{\mathbb{R}^{2N}} \prod_{j=0}^{N-1} \frac{dx_j dq_j}{2\pi} e^{\epsilon \sum_{j=0}^{M-1} \left(\mathcal{H}(x_{j+1}, iq_j) - iq_j \frac{x_j - x_{j+1}}{\epsilon} \right)} \\ &\quad \times |G(t_0)\rangle_{x_0} + O(\epsilon^2) \\ &= \int_{[t_0}^t \mathcal{D}[x, q] e^{-\mathcal{S}[x, iq]} |G(t_0)\rangle_{x_0} \end{aligned}$$

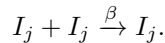
where in the last equation we have taken the continuous limit by introducing the measure

$$\int_{[t_0}^t \mathcal{D}[x, q] = \lim_{N \rightarrow \infty} \int_{\mathbb{R}^{2N}} \prod_{i=0}^{N-1} \frac{dx_i dq_i}{2\pi},$$

and \mathcal{S} is the action defined by Eq. (12). For the multidimensional case the derivation is trivially the same.

Appendix B: WKB approximation for CRNs

Here, we follow the reasoning of [26] and demonstrate that similar arguments can be applied for extend the WKB to the case of chemical reaction networks (3) as well. Let us denote by ω_k the transition rate related to the reaction between k reagents, and by N the total population in the system. For illustrative purposes, let us consider a simple contact process



The transition rate is proportional to the number of elements, n_j , times the probability of finding another element in the heterogeneous network, $(n_i - 1)/N$. Thus, assuming $n_j, N \gg 0$ and $n_j \ll N$, we have $\omega_2(\mathbf{n} - \mathbb{I}_j|\mathbf{n}) = \beta n_j(n_j - 1)/N \propto n_j^2/N$. Generalizing the same reasoning for a contact process between k elements, the transition rate is $\omega_k \propto n_j^k/N^{k-1}$. Since the Doi-Peliti Hamiltonian is a polynomial function of x_j and iq_j , we

conclude that the term related to the highest power of iq_j inside \mathcal{H} is proportional to $(iq_h)^k N^{-k+1}$ ($= N^{-k+1} \partial_{x_j}^k$). Furthermore, with these rates we can write the DPH and the action (12) as extensive quantities with respect to N as done in [26]. If we define the concentration variables $\eta_j = n_j/N$, then the transition rate reads

$$\omega_k \approx \beta \eta_j^k N.$$

By means of Eq. (2) and Eq. (8), we see that

$$H_{n,m} = N h_{m,m}(\eta), \quad \mathcal{S} = N s(\eta),$$

with $\{h_{n,m}\}_{n,m}$ and s being functions of the concentrations only. Using the ansatz $|G\rangle = \exp(-Ns)$, we obtain

$$\frac{\partial_{x_j}^k \exp(-Ns)}{N^{k-1}} = N(-\partial_{x_j} s)^k + O(1) \approx N(-\partial_{x_j} s)^k.$$

Inserting the same ansatz in Eq. (7), the relation $iq_j = -\partial_{x_j} \mathcal{S}$ holds for any j and we find the Hamilton-Jacobi equation

$$\partial_t \mathcal{S} = -\mathcal{H}(\mathbf{x}, -\partial_{\mathbf{x}} \mathcal{S}), \quad (\text{B1})$$

with $\partial_{\mathbf{x}} \mathcal{S} = (\partial_{x_1} \mathcal{S}, \partial_{x_2} \mathcal{S}, \dots)$. Therefore, for CRNs we can always take the stationary action defined by the solutions of Eq.(13) and $|G\rangle = \exp(-\mathcal{S})$.

Appendix C: A basis for the stationary paths

Now we report the basis for the WKB approximation presented in [24]. Considering the one-dimensional case and denoting with $\tilde{x}(t)$ and $\tilde{q}(t)$ the solutions of the Hamilton's equations (13), we take the following basis

$$\begin{aligned} |\tilde{n}\rangle &= (\Delta x + \tilde{x}(t))^n e^{-\tilde{q}(t)(\Delta x + \tilde{x}(t))} \\ \langle \tilde{n}| &= (\partial_{\Delta x} + \tilde{q}(t))^n, \end{aligned}$$

where Δx and $i\Delta q$ are fluctuations of $x(t)$ and $iq(t)$ around the stationary trajectories. The creation and annihilation operators act according to

$$a |\tilde{n}\rangle = n |\tilde{n} - 1\rangle = (\partial_x + \tilde{q}(t)) |\tilde{n}\rangle \quad (\text{C1})$$

$$a^\dagger |\tilde{n}\rangle = |\tilde{n} + 1\rangle = (x + \tilde{x}(t)) |\tilde{n}\rangle. \quad (\text{C2})$$

With this basis, in the derivation of the path integral representation we still have to include the contribution resulting from the time dependency of $|\tilde{n}\rangle$. For the sake of simplicity, we write $\tilde{x}(t) = \tilde{x}$ and $\tilde{q}(t) = \tilde{q}$, and by taking the time derivative of $|\tilde{n}\rangle$ we have

$$\begin{aligned} \partial_t |\tilde{n}\rangle &= \left[n \partial_t \tilde{x} (\Delta x + \tilde{x}^{n-1}) \right. \\ &\quad \left. - (\Delta x + \tilde{x})^n (\partial_t \tilde{q} (\Delta x + \tilde{x}) + \tilde{q} \partial_t \tilde{x}) \right] e^{-\tilde{q}(\Delta x + \tilde{x})} \\ &= n \partial_t \tilde{x} |\tilde{n} - 1\rangle - (\partial_t \tilde{q} (\Delta x + \tilde{x}) + \tilde{q} \partial_t \tilde{x}) |\tilde{n}\rangle \\ &= (\partial_t \tilde{x} a - \partial_t \tilde{q} a^\dagger - \tilde{q} \partial_t \tilde{x}) |\tilde{n}\rangle \\ &=: \mathcal{B} |\tilde{n}\rangle \end{aligned} \quad (\text{C3})$$

where \mathcal{B} is the time evolution operator of the basis. Within this representation, the ME (1) becomes

$$\partial_t |G\rangle = (\mathcal{H} + \mathcal{B}) |G\rangle.$$

Now, by replacing (x, iq) by $(\Delta x, i\Delta q)$, and by substituting \mathcal{H} with $\mathcal{H} + \mathcal{B}$ in the steps presented of Appendix A, we obtain the path integral representation with this new basis. In detail, the action reads

$$\begin{aligned} & -\mathcal{S}[\tilde{x} + \Delta x, \tilde{q} + i\Delta q] \\ &= \int_{t_0}^t d\tau i\Delta q \partial_\tau \Delta x + \mathcal{H}(\tilde{x} + \Delta x, \tilde{q} + i\Delta q) \quad (\text{C4}) \\ & \quad + \mathcal{B}(\tilde{x} + \Delta x, \tilde{q} + i\Delta q) \\ &= \int_{t_0}^t d\tau \left[i\Delta q \partial_\tau \Delta x + \mathcal{H}(\tilde{x}, \tilde{q}) + \Delta x \partial_{\Delta x} \mathcal{H}(\tilde{x}, \tilde{q}) \right. \\ & \quad \left. + i\Delta q \partial_{i\Delta q} \mathcal{H}(\tilde{x}, \tilde{q}) + \Delta \mathcal{H} + \tilde{q} \partial_\tau \tilde{x} + i\Delta q \partial_\tau \tilde{x} \right. \\ & \quad \left. - \Delta x \partial_\tau \tilde{q} - \tilde{x} \partial_\tau \tilde{q} - \tilde{q} \partial_\tau \tilde{x} \right] \\ &= \int_{t_0}^t d\tau \left[i\Delta q \partial_\tau \Delta x + \mathcal{H}(\tilde{x}, \tilde{q}) + \Delta x \partial_\tau \tilde{q} - i\Delta q \partial_\tau \tilde{x} \right. \\ & \quad \left. + \Delta \mathcal{H} + i\Delta q \partial_\tau \tilde{x} - \Delta x \partial_\tau \tilde{q} - \tilde{x} \partial_\tau \tilde{q} \right] \\ &= \int_{t_0}^t d\tau \left[\mathcal{H}(\tilde{x}, \tilde{q}) + \tilde{q} \partial_\tau \tilde{x} \right] - \tilde{x}(t) \tilde{q}(t) + \tilde{x}_0 \tilde{q}_0 \\ & \quad + \int_{t_0}^t d\tau \left[i\Delta q \partial_\tau \Delta x + \Delta \mathcal{H} \right] \\ &= -\tilde{\mathcal{S}} - \tilde{x}(t) \tilde{q}(t) + \tilde{x}_0 \tilde{q}_0 \\ & \quad + \int_{t_0}^t d\tau \left[i\Delta q \partial_\tau \Delta x + \Delta \mathcal{H} \right] \quad (\text{C5}) \end{aligned}$$

where in the second equality we have expanded $\mathcal{H}(\tilde{x} + \Delta x, \tilde{q} + i\Delta q)$ around the stationary trajectories, and $\Delta \mathcal{H}$ includes all the contributions of order $O(\Delta x^2, \Delta q^2, \Delta x \Delta q)$. Here $\tilde{\mathcal{S}}$ satisfies the Hamilton-Jacobi equation (B1).

Let us now rewrite the generating function in terms of the basis $|\tilde{n}\rangle$,

$$|G(t)\rangle_x = e^{\tilde{x}(t)\tilde{q}(t)} \sum_n p(n, t) |\tilde{n}\rangle \Big|_{\Delta x=0}.$$

Thus, the path integral expression is

$$\begin{aligned} & |G(t)\rangle_x = \\ & e^{-\tilde{\mathcal{S}}} \int_{t_0}^t \mathcal{D}[\Delta x, \Delta q] e^{\int_{t_0}^t d\tau (i\Delta q \partial_\tau \Delta x + \Delta \mathcal{H})} |n_0\rangle \Big|_{\substack{\Delta x(t)=0 \\ \tilde{x}(t)=x}} \end{aligned}$$

If we assume fixed initial condition, then $|n\rangle_0 = |\tilde{n}_0\rangle e^{\tilde{x}_0 \tilde{q}_0} = e^{n_0 \log \tilde{x}_0}$. Within the WKB approximation, the fluctuating part does not contribute and we have $|G\rangle = \exp(-\tilde{\mathcal{S}})$ where x and iq are replaced by the real trajectories \tilde{x} and \tilde{q} .

Appendix D: Doi-Peliti Hamiltonian for Complex Reaction Networks

In this section, we present the generic structure of a DPH in the case of chemical reaction networks, providing a proof of the relation (23). For the systems treated in this work, we can distinguish five fundamental processes and, for each of them, we associate a term of the DPH by using definitions (5) and (8). These read

$$\begin{array}{ll} \emptyset \rightarrow A & a_A^\dagger - 1 \\ A \rightarrow 2A & a_A^\dagger (a_A^\dagger - 1) a_A \\ A \rightarrow \emptyset & (1 - a_A^\dagger) a_A \\ A \rightarrow B & (a_A^\dagger - a_B^\dagger) a_A \\ A + B \rightarrow A + C & a_A^\dagger (a_C^\dagger - a_B^\dagger) a_A a_B. \end{array}$$

These derivations can easily be generalized by more complicated interactions such as the ones introduced in Sec. IV B. For a CRN, generally we can build the DPH as a summation of the elements presented above.

Knowing the structure of the DPH, we can now prove Eq. (23). For a two-compartment model, the Kramers-Moyal expansion of the ME reads

$$\partial_t p(\mathbf{n}, t) = \sum_{\substack{m_1, m_2 \\ m_1 + m_2 > 0}} \frac{1}{m_1! m_2!} \partial_{y_1}^{m_1} \partial_{y_2}^{m_2} W^{m_1, m_2}(\mathbf{n}) p(\mathbf{n}, t),$$

where

$$W^{m_1, m_2}(\mathbf{n}) = \int dy_1 dy_2 \omega(\mathbf{n} + y_1 + y_2 | \mathbf{n}) y_1^{m_1} y_2^{m_2}.$$

Taking a two-body interaction

$$pA + qB \xrightarrow{\gamma} (p+k)A + (q-l)B,$$

the transition rate can be written as

$$\omega(\mathbf{n} + y_1 + y_2 | \mathbf{n}) = \gamma n_A^p n_B^q \delta(y_1 + k) \delta(y_2 + l). \quad (\text{D1})$$

Hence

$$W^{m_1, m_2}(\mathbf{n}) = \gamma n_A^p n_B^q k^{m_1} (-l)^{m_2},$$

and we find an expression for \mathcal{H}_{KM}^\dagger

$$\begin{aligned} \mathcal{H}_{KM}^\dagger(\boldsymbol{\eta}, \mathbf{i}\boldsymbol{\theta}) &= \sum_{\substack{m_1, m_2 \\ m_1 + m_2 > 0}} \frac{(i\theta_1 k)^{m_1} (-i\theta_2 l)^{m_2}}{m_1! m_2!} \gamma n_A^p n_B^q \\ &= \gamma n_A^p n_B^q (e^{i\theta_1 k - i\theta_2 l} - 1) \end{aligned} \quad (\text{D2})$$

On the other hand, the DPH for this reaction is

$$\begin{aligned} \mathcal{H} &= \gamma (a_A^\dagger)^p (a_B^\dagger)^{q-l} \left((a_A^\dagger)^k - (a_B^\dagger)^l \right) a_A^p a_B^q \\ &= \gamma \left((a_A^\dagger)^k (a_B^\dagger)^{-l} - 1 \right) (a_A^\dagger)^p a_A^p (a_B^\dagger)^q a_B^q \end{aligned} \quad (\text{D3})$$

By applying the Cole-Hopf transformation, we substitute $a_{A,B}^\dagger = e^{i\theta_{A,B}}$ and $a_{A,B} = e^{-i\theta_{A,B}} \eta_{A,B}$ into Eq. (D3) obtaining the same expression of the Kramers-Moyal expansion (D2). These arguments can be extended to a more complex and general interactions

$$\sum_{i=1}^M p_i I_i \xrightarrow{\gamma} \sum_{i=1}^M (p_i + k_i) I_i,$$

with M representing the number of reagents/compartments $\{I_i\}$ and k_i can be any integer. In this case we define the vector $\mathbf{k} = (k_1, k_2, \dots, k_M)$ and the transition rate is given by

$$\omega(\mathbf{n} + \mathbf{y} | \mathbf{n}) = f(\mathbf{n}) \prod_{j=1}^M \delta(y_j - k_j),$$

where f a suitable function of the occupation numbers. Thus

$$\begin{aligned} W^{m_1, m_2, \dots, m_M}(\mathbf{n}) &= \int d\mathbf{y} \left(\prod_{j=1}^M y_j^{m_j} \right) \omega(\mathbf{n} + \mathbf{y} | \mathbf{n}) f(\mathbf{n}) \\ &= f(\mathbf{n}) \prod_{j=1}^M k_j^{m_j}, \end{aligned}$$

and the adjoint of the Kramers-Moyal operator is

$$\begin{aligned} \mathcal{H}_{KM}^\dagger(\boldsymbol{\eta}, \mathbf{i}\boldsymbol{\theta}) &= \sum_{\substack{m_1, m_2, \dots, m_M \\ \sum_j m_j > 0}} \prod_{j=1}^M \frac{(i\theta_j k_j)^{m_j}}{m_j!} f(\boldsymbol{\eta}) \\ &= \left(\prod_{j=1}^M e^{i\theta_j k_j} - 1 \right) f(\boldsymbol{\eta}). \end{aligned} \quad (\text{D4})$$

In terms of the Doi-Peliti representation, the corresponding DPH is

$$\mathcal{H} = \gamma \sum_{i=1}^M \left((a_i^\dagger)^{k_i} - 1 \right) f(a^\dagger a), \quad (\text{D5})$$

which can also be written as a function of the Cole-Hopf variables,

$$\mathcal{H}(\boldsymbol{\eta}, \mathbf{i}\boldsymbol{\theta}) = \gamma \left(\prod_{j=1}^M e^{i\theta_j k_j} - 1 \right) f(\boldsymbol{\eta}).$$

This is equal to the KM operator (D4). Eq. (D5) shows that the mean-field manifold $\mathbf{q} = 0$ ($\boldsymbol{\theta} = 0$) is always a zero of \mathcal{H} .

By means of the relation (23), we can show the link with the Langevin equation (25). The procedure for deriving Langevin dynamics from \mathcal{H}_{KM} has been discussed in several works (e.g. [24] and [27]) and, for completeness, we sketch the derivation in the following.

In the simple one-dimensional case, we can develop a path-integral representation of the probability distribution starting from the Kramers-Moyal expansion (21). Following the same steps reported in Appendix A, we write

$$p(n, t) = \int_{[0}^t \mathcal{D}[\eta, \theta] e^{-\mathcal{S}_{KM}^\dagger[\eta, \theta]} \delta(n - \eta(t)),$$

where the action is defined by

$$\mathcal{S}_{KM}^\dagger = \int_0^t d\tau i\theta(\tau) \partial_\tau \eta(\tau) - \mathcal{H}_{KM}^\dagger(\eta(\tau), i\theta(\tau)).$$

As discussed in the main text, we know that the deterministic limit is recovered for $\theta \rightarrow 0$. To obtain the Langevin expression, we expand \mathcal{S}^\dagger around $\theta = 0$ up to the second order and integrate with respect $\theta(\tau)$,

$$p(n, t) = \int_{[0}^t \mathcal{D}[\eta] e^{-\int_0^t \frac{(\partial_\tau \eta - \partial_\theta \mathcal{H}_{KM}^\dagger|_{\theta=0})^2}{2\partial_\theta^2 \mathcal{H}_{KM}^\dagger|_{\theta=0}} d\tau} \delta(n - \eta(t)),$$

where $\mathcal{D}[\eta]$ is the re-normalized measure. The latter expression is nothing but the Feynman-Kac formula [24]

$$p(n, t) = \langle \delta(n - \eta(t)) \rangle_\eta,$$

where $\langle \cdot \rangle_\eta$ is the average over the trajectories defined by

$$\frac{d\eta(t)}{dt} = \partial_\theta \mathcal{H}_{KM}^\dagger|_{\theta=0} + \sqrt{\partial_\theta^2 \mathcal{H}_{KM}^\dagger|_{\theta=0}} \cdot \xi(t)$$

where $\xi(t)$ is the standard white noise. Including the relation (23), we recover Eq. (25). The generalization to the multidimensional case is straightforward.

Appendix E: Closure transition rates

Here we discuss some limits of our formalism. In the main text, we have considered models such as the *SIS* or *SIRS* that have a closed diagrammatic structure, and systems where each compartment is subject to at least two interactions. Indeed, as we will show, these features provide the necessary conditions to apply the Doi-Peliti mapping.

Let us take a chemical reaction model with M compartments $\{I_1, I_2, \dots, I_M\}$ and where only spontaneous transitions and contact interactions occur. We assume I_M is connected to other compartments by a single spontaneous transition $I_j \xrightarrow{\gamma} I_M$. Thus, I_M is a termination of the model diagram. Moreover, we consider to work with fixed N and, as for the *SIS* model, we take $I_1 \approx N$. We choose the order parameter ρ as in Eq. (17). Now, we focus on I_1 and I_M to understand if and when a phase transition occurs. We rewrite the diagram of the system as where we have replaced the $M - 2$ compartments I_2, \dots, I_{M-1} by an effective one I_{eff} . The effective transition rates ω_{I_1} and $\omega_{I_{\text{eff}}}$ are functions of all populations

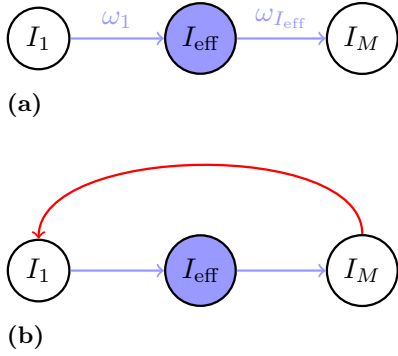


Fig. A1: *SIR*-like diagram for the effective *open* process (a) and *SIRS*-like diagram for the effective *closed* process (b).

except n_M . Thus, the system is active when I_{eff} becomes asymptotically populated and we can write

$$\partial_t \langle n_{I_{\text{eff}}} \rangle(t) = f(\{\beta\}, I_1, I_{\text{eff}}), \quad (\text{E1})$$

with $\{\beta\}$ representing the transition coefficients of the model, and f is a suitable function depending on the system we are considering. The problem is that the mean-field equations include

$$\partial_t \langle n_M \rangle = \gamma \langle n_j \rangle, \quad (\text{E2})$$

from which, at the stationary limit, $\langle n_j \rangle = 0$. The presence of null terms like this leads to a degeneration of the system (19). Thus $\det(\mathbf{J}) = 0$ for any fixed point and we cannot use the strategy presented in the main text to analyse the critical behaviour. To overcome this problem, we introduce an effective transition rate that closes the model diagram connecting I_M directly to I_1 by means of a spontaneous transition $\omega(\mathbf{n} - \mathbb{I}_M + \mathbb{I}_{I_1} | \mathbf{n})$. In doing so we obtain a *SIRS*-like model, as depicted in A1b.

From now on we will call *open* a system described by diagrams like Fig. A1a, and *closed* a system represented by diagrams like Fig. A1b. By following a classical treatment [13], one can prove that both the *SIR* and *SIRS* models, have the same critical condition. Indeed, both of them are active when the number of elements in state I grows during the early stage of the process. For $t \approx 0$ we have $n_S \approx N$, and from the mean-field equations it is easy to find the critical condition

$$\partial_t \langle n_I \rangle = \frac{\beta}{N} \langle n_I \rangle \langle n_S \rangle - \gamma \langle n_I \rangle \approx (\beta - \gamma) \langle n_I \rangle \quad (\text{E3})$$

Therefore, the epidemic spreads when initially the population of infected individuals manages to grow fast enough, that is, when $\beta > \gamma$. Since Eq. (E3) holds for both *SIR* and *SIRS*, we have that the critical condition does not change.

Focusing back on a general process, we can repeat the same steps to find that

$$\partial_t \langle n_{I_{\text{eff}}} \rangle(t) = f(\{\beta\}, I_1, I_{\text{eff}}),$$

where $\{\beta\}$ are the transition coefficients of the *SIR*-like process, and f is a suitable function depending on the system we are considering. As for the *SIR* and *SIRS* models, by assuming $I_1 \approx N$ for $t \approx 0$, the critical behavior is defined by the system

$$\begin{cases} \partial_t \langle n_{I_{\text{eff}}} \rangle = f(\{\beta\}, I_{\text{eff}}) \\ \partial_t \langle n_M \rangle = \epsilon \langle n_j \rangle \end{cases}, \quad (\text{E4})$$

where we are assuming that $I_j \in I_{\text{eff}}$ is the only compartment linked to the termination I_M by a spontaneous transition with per capita rate $\epsilon > 0$. As we will show below, these arguments can be generalized for system with several terminations. As for the *SIRS* model, by adding a re-filling reaction $\omega(\mathbf{n} - \mathbb{I}_M + \mathbb{I}_{I_1}, \mathbf{n}) = \sigma I_M$, the system (E4) becomes

$$\begin{cases} \partial_t \langle n_{I_{\text{eff}}} \rangle = f(\{\beta\}, I_{\text{eff}}) \\ \partial_t \langle I_M \rangle = \epsilon \langle I_j \rangle - \sigma \langle I_M \rangle \end{cases}.$$

Since the phase transition occurs when the I_{eff} becomes active, the critical condition is independent of I_M and it is determined by the first equation. Thus, we conclude that the critical condition for such system is the same of the corresponding closed diagram. We can generalize these arguments to more complex systems by imposing only two conditions

1. each extremity of the open diagram is linked to the main process by a spontaneous transition;
2. the closed diagram is given by adding spontaneous transitions from the extremity to the initial empty state.

The first condition ensures the inner part of the process is independent of the population numbers of the extremities². The second condition guarantees to have the same diagrammatic structure of the *SIRS* model.

Appendix F: Further examples of models studied through the dimension reduction

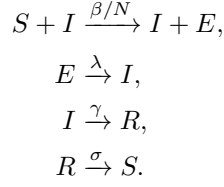
With the aim of showing the depth and breadth of our formalism, we discuss in this Appendix section its application to a variety of models not treated in the main text.

1. The standard *SEIRS* model

We start with the usual *SEIRS* model, where the spread of a disease is assumed to occur by mean of 4

² For example, with pair interactions, $f(\{\beta\})$ would depend on the population of the ends.

compartments. Individuals can be in one of the susceptible S , incubation E , infected I and recovered R states. The model is defined by the following transition rates:



In this case we are considering a system with a fixed total population N , and we consider $n_S(0) \approx N$. Therefore, according to the notation introduced above, $S = I_1$. The Doi-Peliti Hamiltonian for this model is

$$\begin{aligned} \mathcal{H} = &\frac{\beta}{N}(a_E^\dagger - a_S^\dagger)a_S a_I^\dagger a_I + \lambda(a_I^\dagger - a_E^\dagger)a_E + \\ &+ \gamma(a_R^\dagger - a_I^\dagger)a_I + \sigma(a_S^\dagger - a_R^\dagger)a_R, \end{aligned}$$

and the mean-field trajectories are

$$\begin{aligned} \partial_t \langle n_S \rangle &= -\frac{\beta}{N} \langle n_S \rangle \langle n_I \rangle + \sigma \langle n_R \rangle, \\ \partial_t \langle n_E \rangle &= \frac{\beta}{N} \langle n_S \rangle \langle n_I \rangle - \lambda \langle n_E \rangle, \\ \partial_t \langle n_I \rangle &= \lambda \langle n_E \rangle - \gamma \langle n_I \rangle, \\ \partial_t \langle n_R \rangle &= \gamma \langle n_I \rangle - \sigma \langle n_R \rangle. \end{aligned} \quad (\text{F1})$$

By setting the last two equations equal to zero, and by taking into account the conservation of total (normalized) population $1 = x_S q_S + q_E + q_I + q_R$, we find the following parameterization

$$\begin{aligned} x_E = x_I = x_R = 1, \quad q_E &= -\frac{\beta\sigma(x_S q_S - 1)q_S}{\gamma\lambda + \lambda\sigma + \beta\sigma q_S}, \\ q_I &= \frac{\lambda\sigma(x_S q_S - 1)}{\gamma\lambda + \lambda\sigma + \beta\sigma q_S}, \quad q_R = \frac{\lambda\gamma(x_S q_S - 1)}{\gamma\lambda + \lambda\sigma + \beta\sigma q_S}. \end{aligned}$$

By putting these expressions into the DPH, we obtain the reduced Hamiltonian in the CH representation

$$\mathcal{H}^* = \frac{(1-\eta)e^{-\theta}(e^\theta - 1)\lambda\sigma(\gamma e^\theta - \beta\eta)}{\gamma(\lambda + \sigma) + \lambda\sigma}.$$

Three zero-energy lines are found, namely,

$$\eta = 1, \quad \theta = 0, \quad \theta = \Theta(\eta) = \log(\eta\beta/\gamma).$$

The absorbing phase, where the disease gets extinct, corresponds to $(1, 0)$ on the plane (η, θ) . By plotting these lines, we observe in Fig. (A2) the well-known phase transition for the *SEIRS* model at $\beta = \gamma$. Since no new fixed points appear, we identify it as a second-order

transition, as expected. We can choose different ways to define the parametrization, that is we have several possible Λ with different reduced DPHs. In this particular case, the zero energy phase portraits of the different Hamiltonians are identical. In the next section we will show an example in which the degeneration of Λ leads to have different phase portraits.

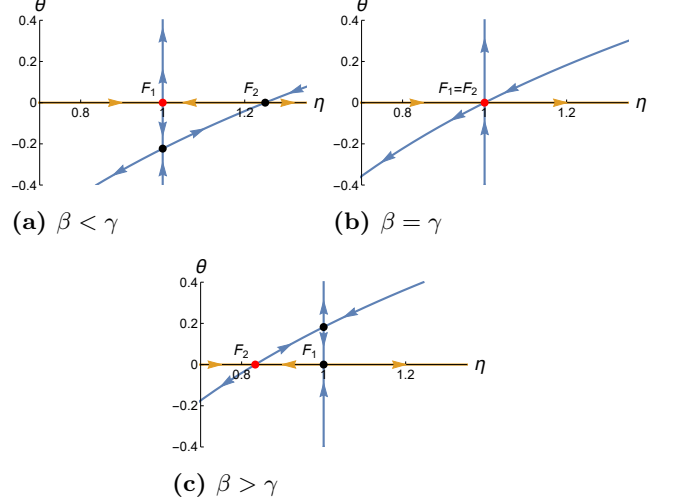
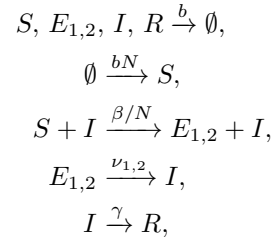


Fig. A2: Identifying phase transitions in the *SEIRS* model. Panels A2a, A2b and A2c show the phase portrait of the reduced system by varying β/γ . The orange curves represent the deterministic trajectories, while the blue ones are the non-trivial energy lines. Black and red dots represent the fixed points on the mean-field manifold. In particular the red ones are the attractors of the dynamics. At the critical point, $\beta = \gamma$, the attractor changes smoothly and we observe a second-order phase transition.

2. *SEIR* model with two latent categories

Now we study the epidemiological model discussed in [15] by means of the next-generation matrix method [14]. This model is an extension of the *SEIR*, where two latent categories E_1 and E_2 are considered. The transition rates are



where $p_1 = p$ and $p_2 = 1 - p$. Its DPH reads

$$\begin{aligned} \mathcal{H} = & bN(a_S^\dagger - 1) + b \left[(1 - a_S^\dagger)a_S + (1 - a_{E_1}^\dagger)a_{E_1} + (1 - a_{E_2}^\dagger)a_{E_2} + (1 - a_I^\dagger)a_I + (1 - a_R^\dagger)a_R \right] \\ & + p\beta \frac{(a_{E_1}^\dagger - a_S^\dagger)a_I^\dagger a_I a_S}{N} + \beta(1-p) \frac{(a_{E_2}^\dagger - a_S^\dagger)a_I^\dagger a_I a_S}{N} + \nu_1(a_I^\dagger - a_{E_1}^\dagger)a_{E_1} + \nu_2(a_I^\dagger - a_{E_2}^\dagger)a_{E_2} + \gamma(a_R^\dagger - a_I^\dagger)a_I \quad (\text{F2}) \end{aligned}$$

By means of the Hamilton's equations related to (F2), the differential equations for the deterministic trajectories are

$$\begin{aligned} \partial_t \langle n_S \rangle &= -\beta \frac{\langle n_S \rangle \langle n_I \rangle}{N} + Nb - \langle n_S \rangle b \\ \partial_t \langle n_{E_{1,2}} \rangle &= p_{1,2} \beta \frac{\langle n_S \rangle \langle n_I \rangle}{N} - (b + \nu_{1,2}) \langle n_{E_{1,2}} \rangle \\ \partial_t \langle n_I \rangle &= -(\gamma + b) \langle n_I \rangle + \nu_1 \langle n_{E_1} \rangle + \nu_2 \langle n_{E_2} \rangle \\ \partial_t \langle n_R \rangle &= \gamma \langle n_I \rangle - b \langle n_R \rangle \end{aligned}$$

By setting the last three equations equal to 0, and taking into account conservation of number of particles N , we find the following transformations (renormalized with respect to N):

$$\begin{aligned} q_{E_1} &= -\frac{b(x_S q_S - 1) [(\gamma + b)(b + \nu_2) + \beta \nu_2 (p - 1) q_S]}{(\gamma + b)(b + \nu_1)(b + \nu_2) - \beta b (p - 1) q_S (\nu_1 - \nu_2)} \\ q_{E_2} &= \frac{\beta b \nu_1 (p - 1) q_S (x_S q_S - 1)}{(\gamma + b)(b + \nu_1)(b + \nu_2) - \beta b (p - 1) q_S (\nu_1 - \nu_2)} \\ q_I &= -\frac{b \nu_1 (b + \nu_2) (x_S q_S - 1)}{(\gamma + b)(b + \nu_1)(b + \nu_2) - \beta b (p - 1) q_S (\nu_1 - \nu_2)} \\ q_R &= -\frac{\gamma \nu_1 (b + \nu_2) (x_S q_S - 1)}{(\gamma + b)(b + \nu_1)(b + \nu_2) - \beta b (p - 1) q_S (\nu_1 - \nu_2)} \end{aligned}$$

These equations define the map Λ from which we derive the reduced Hamiltonian

$$\begin{aligned} \mathcal{H}^* = & b \left[\eta (e^{-\theta} - 1) + e^\theta - 1 + \right. \\ & \left. - \frac{\beta \eta (e^\theta - 1) \nu_1 (\eta - 1) (b + \nu_2)}{\beta b (p - 1) \eta (\nu_1 - \nu_2) - e^\theta (\gamma + b) (b + \nu_1) (b + \nu_2)} \right] \end{aligned}$$

By solving Eqs. (19), we see that two different hyperbolic points overlap for

$$\tilde{\beta} = \frac{(\gamma + b)(b + \nu_1)(b + \nu_2)}{b\nu_2 + \nu_1\nu_2 + b\nu_1 p - b\nu_2 p}, \quad (\text{F3})$$

which is the same result obtained by the next-generation matrix [15]. The phase portraits are reported in Fig. (A3). From Figs. A3a, A3b and A3c, we see that at the critical condition no new hyperbolic fixed points appear, therefore the phase transition is of the second-order as verified by the numerical simulations (Fig. A3d).

As discussed in the main text, since we have the population conservation as first integral, there is an arbitrariness in the derivation of Λ . In this case, in addition to the parametrization presented before, we have

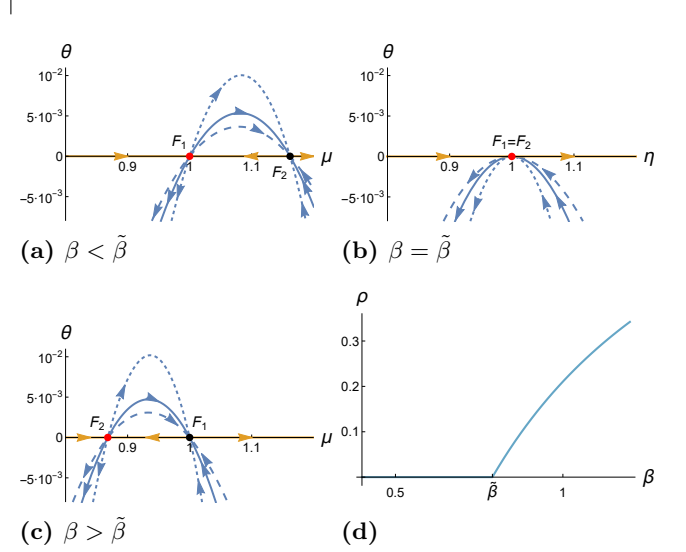


Fig. A3: Phase transition for the SEIR with two latent categories. Panels A3a, A3b and A3c show the phase portrait of the reduced system, where the blue line is the mean-field manifold and the orange ones are the non-trivial zero-energy levels. The dashed lines represent the different parameterizations. Black and red dots represent the fixed points on the mean-field manifold. In particular, the red ones are the attractors of the dynamics. Panel A3d shows the dependence of the order parameter as a function of β , from numerical simulation. We have considered: $b = 0.2$, $\gamma = 0.3$, $p = 0.9$, $\nu_1 = 0.4$ and $\nu_2 = 0.1$. Therefore, the phase transition occurs at $\tilde{\beta} = 0.7895$.

studied two others Λ_2 and Λ_3 . Choosing as first integrals the conservation of N , the second, the fourth and the fifth deterministic equations we obtain Λ_2 , while by taking the N conservation with the second, the third and the fifth equations we have Λ_3 . The phase portrait of the corresponding reduced Hamiltonians is represented in Fig. (A3). We have analyzed the long-time behavior of the different Langevin dynamics (25). For each equation, we have performed a simulation in the active phase and compared the stationary distribution for n_S . The results are shown in Fig. (A4). Distributions show differences as expected, however they have the identical average and provide a qualitative description of the stochastic environment of the system. Further studies are needed to research a criterion for selecting only one parameterization over the others.

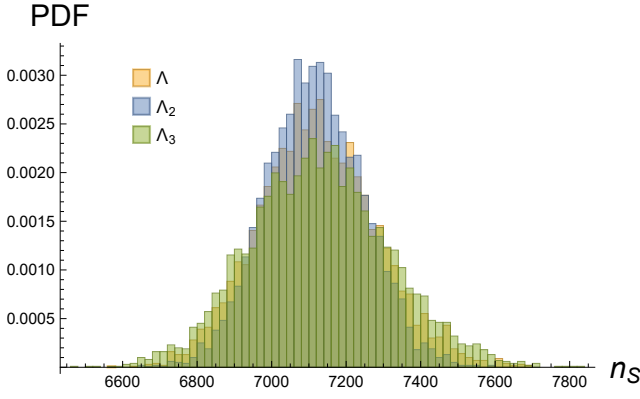
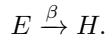
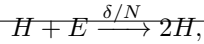
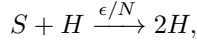
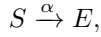
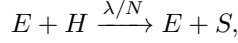


Fig. A4: Numerical asymptotic distribution of the susceptible individuals for the *SEIR* model with two latent categories. The different colors represent the three different parametrizations: Λ , Λ_2 and Λ_3 . We have considered $N = 10^4$, $\beta = 1.11$, $b = 0.2$, $\nu_1 = 0.4$, $\nu_2 = 0.1$, $p = 0.9$ and $\gamma = 0.3$. In this case, the critical point is $\tilde{\beta} = 0.7895$.

3. Tax evasion model

We analyse with our formalism a simple model for tax evasion that undergoes first-order phase transitions [63]. The model includes 3 compartments: honest individuals H , susceptible ones S and evaders E . The dynamics are described by the following elementary reactions,



$$\eta \equiv 1, \quad \theta = \Theta(\eta) = \log \left(\eta \frac{\sqrt{(-\alpha\lambda + \beta\epsilon + \delta\eta\epsilon + \eta\lambda\epsilon)^2 + 4\alpha\lambda\epsilon(\beta + \delta\eta)} + \alpha\lambda - \beta\epsilon - \delta\eta\epsilon - \eta\lambda\epsilon}{2\alpha(\beta + \delta\eta)} \right).$$

We denote by F_- and F_+ the intersection of Θ with the mean-field line, where $\eta_{F_-} \leq \eta_{F_+}$, and $F_1 = (1, 0)$ is the usual absorbing state (see Fig. A5). By considering λ as control parameter, we find that $\Theta(1) = 0$ for λ equal to

$$\tilde{\lambda} := \frac{(\alpha + \epsilon)(\beta + \delta)}{\alpha}. \quad (\text{F4})$$

For $\lambda < \tilde{\lambda}$, as reported in Figs. A5a and A5d, the system converges to F_1 and there are no phase transition. Moreover, at the critical point, for ϵ equal to

$$\tilde{\epsilon} := \frac{\alpha\beta}{\delta},$$

Θ is tangent to the mean-field line and $F_+ = F_- = (1, 0)$,

The DPH is given by

$$\mathcal{H} = \frac{\epsilon}{N} a_H^\dagger (a_H^\dagger - a_S^\dagger) a_H a_S + \frac{\delta}{N} a_H^\dagger (a_H^\dagger - a_E^\dagger) a_H a_E + \frac{\lambda}{N} a_E^\dagger (a_S^\dagger - a_H^\dagger) a_H a_E + \alpha (a_E^\dagger - a_S^\dagger) a_S + \beta (a_H^\dagger - a_E^\dagger) a_E,$$

and the mean-field equations read

$$\begin{aligned} \partial_t \langle n_H \rangle &= \frac{\epsilon}{N} \langle n_H \rangle \langle n_S \rangle + \beta \langle n_E \rangle + \frac{\delta}{N} \langle n_H \rangle \langle n_E \rangle \\ &\quad - \frac{\lambda}{N} \langle n_H \rangle \langle n_E \rangle \\ \partial_t \langle n_S \rangle &= -\alpha \langle n_S \rangle - \frac{\epsilon}{N} \langle n_H \rangle \langle n_S \rangle + \frac{\lambda}{N} \langle n_H \rangle \langle n_E \rangle \\ \partial_t \langle n_E \rangle &= \alpha \langle n_S \rangle - \beta \langle n_E \rangle - \frac{\delta}{N} \langle n_E \rangle \langle n_H \rangle. \end{aligned}$$

In this model, N is fixed and we consider $\rho = 1 - \lim_{t \rightarrow \infty} \langle n_H \rangle / N$ as the order parameter. After re-scaling the system size to $N = 1$, we take as first integrals the last mean-field equation and the population conservation, obtaining the parametrization

$$q_S = -\frac{\lambda q_H (x_H q_H - 1)}{\alpha + q_H (\lambda + \epsilon)}, \quad q_E = \frac{(\alpha + q_S \epsilon)(1 - x_H q_H)}{\alpha + q_H (\epsilon + \lambda)}.$$

The corresponding reduced Hamiltonian is:

$$\mathcal{H}^* = -\frac{(\eta - 1)e^{-\theta} (e^\theta - 1)}{\alpha e^\theta + \eta(\lambda + \epsilon)} \left(\alpha e^{2\theta} (\beta + \delta\eta) + \eta e^\theta (-\alpha\lambda + \beta\epsilon + \delta\eta\epsilon + \eta\lambda\epsilon) - \eta^2 \lambda \epsilon \right).$$

The zero-energy curves intersecting the mean-field line are

so we find a tricritical point. In particular, for $\epsilon < \tilde{\epsilon}$, at the critical point we find $F_- = (1, 0)$ (Panel A5b). By studying the eigenvalues, we observe that F_- becomes the attractor (Panel A5c) and a second-order phase transition occurs. Otherwise, if $\epsilon > \tilde{\epsilon}$, at $\lambda = \tilde{\lambda}$ we have $F_+ = (1, 0)$ as shown in Fig. A5e and for $\lambda > \tilde{\lambda}$ the dynamics jumps to the new attractor F_- (Fig. A5f). Therefore, there is an abrupt changing of the asymptotic behavior, that is a first-order transition. A picture of this behaviour is reported in Fig. A5 and in Fig. A6 we show a numerical simulation for both the first- and second-order phase transition. We point out that, while the critical value (F4) corresponds to the result predicted in [63], with our method we find a continuous critical behaviour

from low ϵ that had not been investigated before.

4. Levin's model

Let us now study another model of ecological interest widely treated in the literature: the Levin's model. This model is characterized by two types of processes, namely, one of population proliferation in an empty patch, and one of extinction. We focus on systems containing two

species A and B whose dynamics are defined by the rates

$$\begin{aligned}\omega(\mathbf{n} + \mathbb{I}_A - \mathbb{I}_\emptyset, \mathbf{n}) &= \frac{c}{N} n_A (n_\emptyset - D) \\ \omega(\mathbf{n} + \mathbb{I}_B - \mathbb{I}_\emptyset, \mathbf{n}) &= \frac{\beta}{N^2} n_A n_B (n_\emptyset - D) \\ \omega(\mathbf{n} - \mathbb{I}_{A,B} + \mathbb{I}_\emptyset, \mathbf{n}) &= n_{A,B} \epsilon\end{aligned}\quad (\text{F5})$$

where n_\emptyset represents the number of non-occupied patches. Moreover, we are including D patches that have been damaged and can no longer be occupied. The population A has an independent growth, while the dynamics of B depends on A . From these rates, we see that $N \geq n_\emptyset \geq D$ to have a well defined dynamics.

The Doi-Peliti Hamiltonian reads

$$\begin{aligned}\mathcal{H} &= \frac{cD}{N} a_A^\dagger (a_A^\dagger - a_\emptyset^\dagger) a_A a_\emptyset - \frac{cD}{N} a_A^\dagger [(a_\emptyset)^\dagger - 1] a_A + \frac{\beta}{N} (a_B^\dagger - a_\emptyset^\dagger) a_A^\dagger a_B^\dagger a_A a_B a_\emptyset \\ &\quad - \frac{\beta D}{N} [a_B^\dagger (a_\emptyset^\dagger)^{-1} - 1] a_A^\dagger a_B^\dagger a_A a_B + \epsilon (a_\emptyset^\dagger - a_A^\dagger) a_A + \epsilon (a_\emptyset^\dagger - a_B^\dagger) a_B,\end{aligned}$$

and the mean-field equations are

$$\begin{aligned}\partial_t \langle n_A \rangle &= \frac{c}{N} \langle n_A \rangle (\langle n_\emptyset \rangle - D) - \epsilon \langle n_A \rangle \\ \partial_t \langle n_B \rangle &= \frac{\beta}{N^2} \langle n_A \rangle \langle n_B \rangle (\langle n_\emptyset \rangle - D) - \epsilon \langle n_B \rangle \\ \partial_t \langle n_\emptyset \rangle &= -\partial_t \langle n_A \rangle - \partial_t \langle n_B \rangle\end{aligned}$$

We choose $\langle n_A \rangle / N$ as the order parameter and D as the control variable. The solution of (19) yields two critical points

$$\begin{aligned}\text{A)} \quad \frac{\langle n_A \rangle}{N} &= 0, \quad \frac{\langle n_B \rangle}{N} = 0, \quad \frac{\langle n_\emptyset \rangle}{N} = 1, \quad \tilde{D}_1 = N \left(1 - \frac{\epsilon}{c}\right), \\ \text{B)} \quad \frac{\langle n_A \rangle}{N} &= \frac{c}{\beta}, \quad \frac{\langle n_B \rangle}{N} = 0, \quad \frac{\langle n_\emptyset \rangle}{N} = \left(1 - \frac{c}{\beta}\right), \\ &\quad \tilde{D}_2 = N \left(1 - \frac{c}{\beta} - \frac{\epsilon}{c}\right).\end{aligned}$$

Thus $\tilde{D}_1 > \tilde{D}_2$, and we expect to observe two phase transitions. By solving Eq. (18) with the second mean-field equation and the population conservation as constraints, we obtain two parametrizations $\Lambda(x_A, q_A) = (x_A, x_B, x_\emptyset, q_A, q_B, q_\emptyset)$, as in Appendix IV D. They are

$$\begin{aligned}\Lambda^{(A)} &= \\ &\quad \left(x_A, 1, 1, q_A, N - D - q_A x_A - \frac{\epsilon N^2}{q_A \beta}, D + \frac{\epsilon}{q_A \beta}\right), \\ \Lambda^{(B)} &= (x_A, 1, 1, q_A, 0, N - x_A q_A).\end{aligned}$$

We denote by $\mathcal{H}^{*(A)}$ and $\mathcal{H}^{*(B)}$ respectively the reduced Hamiltonians for $\Lambda^{(A)}$ and $\Lambda^{(B)}$, that read

$$\begin{aligned}\mathcal{H}^{*(A)} &= \frac{e^{-\theta} (e^\theta - 1) \epsilon (ce^{2\theta} - \beta\eta)}{\beta} \\ \mathcal{H}^{*(B)} &= -e^{-\theta} (e^\theta - 1) \eta (ce^\theta (d + \eta - 1) + \epsilon),\end{aligned}$$

where we have re-normalized the population with respect to N and we have introduced $d = D/N$. By analysing their zero-energy lines with the attractors of the dynamics, we note that the system is described by $\mathcal{H}^{*(B)}$ for $D < \tilde{D}_1$, and by $\mathcal{H}^{*(A)}$ otherwise. A sketch of the phase portraits is shown in panels A7a, A7b and A7c.

A numerical simulation for the system is reported in panel A7d. There, we can observe 3 regimes, separated by the two phase transitions found above. The first regime, for $D < \tilde{D}_2$, is characterized by the coexistence of both populations. In the second one, for $\tilde{D}_2 < D < \tilde{D}_1$, only population A survives. For $D > \tilde{D}_1$, the fragmentation is too strong and there is complete extinction of all species. In both cases we have a second-order phase transition.

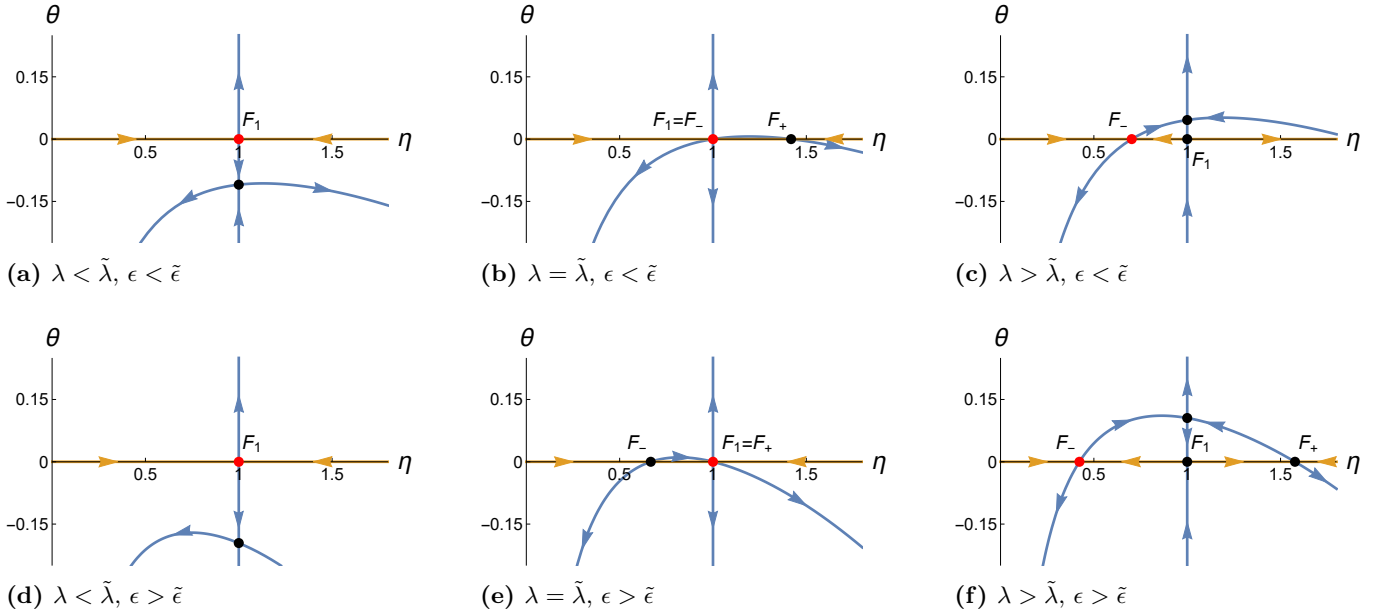


Fig. A5: Phase portrait for the taxes evasion model. The orange lines represent the mean-field manifold, while the blue ones are the other non zero-energy lines. F_1 and F_{\pm} are the system fixed points. Red dots are the attractors of the deterministic dynamics. In the upper Panels A5a, A5b and A5c, we report the second-order phase transition behavior: with $\epsilon < \tilde{\epsilon}$, we see that the intersection F_1 overlaps with F_+ and becomes the new attractor. The asymptotic state changes smoothly and we have a continuous phase transitions. Otherwise, in the lower Panels A5d, A5e and A5f, when $\lambda = \tilde{\lambda}$, we have $F_1 = F_+$ and the dynamics varies in a discontinuous way converging in F_- . So we assist to a first-order phase transitions.

-
- [1] L. Freeman *et al.*, The development of social network analysis, *A Study in the Sociology of Science* **1**, 159 (2004).
- [2] J. M. Montoya, S. L. Pimm, and R. V. Solé, Ecological networks and their fragility, *Nature* **442**, 259 (2006).
- [3] G. Kossinets and D. J. Watts, Empirical analysis of an evolving social network, *Science* **311**, 88 (2006).
- [4] B. D. Fath, U. M. Scharler, R. E. Ulanowicz, and B. Hannon, Ecological network analysis: network construction, *Ecological Modelling* **208**, 49 (2007).
- [5] C. Castellano, S. Fortunato, and V. Loreto, Statistical physics of social dynamics, *Reviews of Modern Physics* **81**, 591 (2009).
- [6] T. C. Ings, J. M. Montoya, J. Bascompte, N. Blüthgen, L. Brown, C. F. Dormann, F. Edwards, D. Figueroa, U. Jacob, J. I. Jones, *et al.*, Ecological networks—beyond food webs, *Journal of Animal Ecology* **78**, 253 (2009).
- [7] J. Bascompte, Structure and dynamics of ecological networks, *Science* **329**, 765 (2010).
- [8] M. De Domenico, A. Lima, P. Mougél, and M. Musolesi, The anatomy of a scientific rumor, *Scientific reports* **3**, 2980 (2013).
- [9] R. Gallotti, F. Valle, N. Castaldo, P. Sacco, and M. De Domenico, Assessing the risks of ‘infodemics’ in response to covid-19 epidemics, *Nature Human Behaviour* **4**, 1285 (2020).
- [10] V. Belik, T. Geisel, and D. Brockmann, Natural human mobility patterns and spatial spread of infectious diseases, *Physical Review X* **1**, 011001 (2011).
- [11] J. Gómez-Gardeñes, D. Soriano-Panos, and A. Arenas, Critical regimes driven by recurrent mobility patterns of reaction–diffusion processes in networks, *Nature Physics* **14**, 391 (2018).
- [12] P. Castioni, R. Gallotti, and M. De Domenico, Critical behavior in interdependent spatial spreading processes with distinct characteristic time scales, *Communications Physics* **4**, 131 (2021).
- [13] R. Pastor-Satorras, C. Castellano, P. Van Mieghem, and A. Vespignani, Epidemic processes in complex networks, *Reviews of Modern Physics* **87**, 925 (2015).
- [14] O. Diekmann, J. A. P. Heesterbeek, and J. A. J. Metz, On the definition and the computation of the basic reproduction ratio R_0 in models for infectious diseases in heterogeneous populations, *Journal of Mathematical Biology* **28**, 365 (1990).
- [15] O. Diekmann, J. Heesterbeek, and M. G. Roberts, The construction of next-generation matrices for compartmental epidemic models, *Journal of the Royal Society Interface* **7**, 873 (2010).
- [16] V. Colizza, R. Pastor-Satorras, and A. Vespignani, Reaction–diffusion processes and metapopulation models in heterogeneous networks, *Nature Physics* **3**, 276 (2007).
- [17] V. Colizza and A. Vespignani, Epidemic modeling in metapopulation systems with heterogeneous coupling pattern: Theory and simulations, *Journal of Theoretical Biology* **251**, 450 (2008).

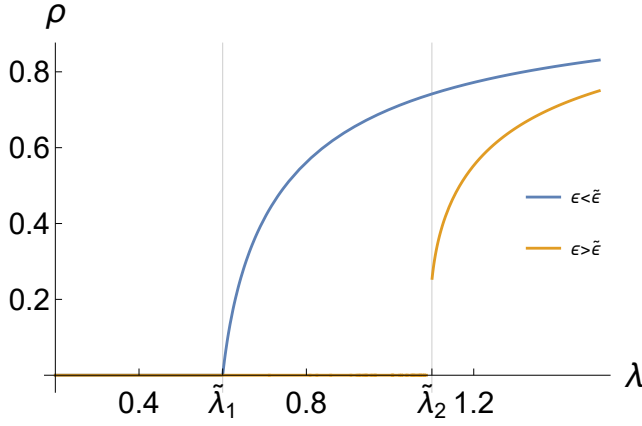


Fig. A6: Numerical asymptotic distribution of the honest individuals. The blue line represents the second order phase transition, while the orange one is the first order transition. For both the cases we have considered: $\beta = 0.2$, $\alpha = 0.3$, $\gamma = 0.1$, thus $\tilde{\epsilon} = 0.6$. For the first order transition instead $\epsilon = 0.8$, hence $\tilde{\lambda} = 1.1$. For the continuous transition instead $\epsilon = 0.3$ and $\tilde{\lambda} = 0.6$.

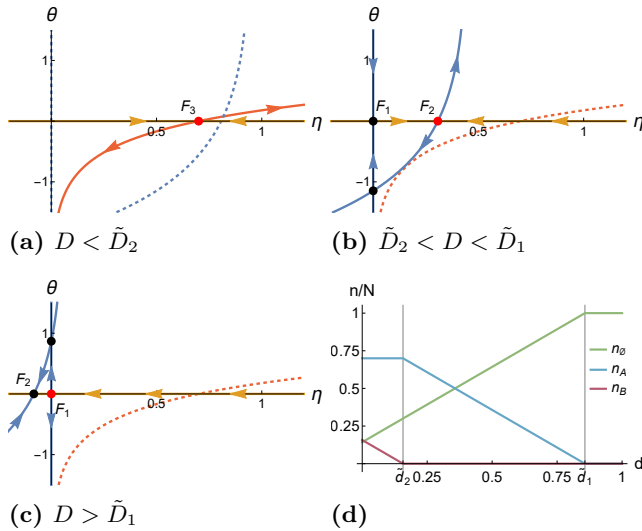


Fig. A7: Phase transition for the Levin's model. Panels A7a, A7b and A7c show the phase portraits of the reduced system, where the orange lines are the mean-field manifold, the red lines are the zero-energy line of $\mathcal{H}^{*(A)}$ and the blue ones are related to $\mathcal{H}^{*(B)}$. Red dots represent the fixed points on the mean-field manifold. Panel A7d is a numerical simulation of the model with $\beta = 1$, $c = 0.7$ and $\epsilon = 0.1$, hence $\tilde{d}_1 = 0.157$ and $\tilde{d}_2 = 0.857$.

[18] S. Gómez, J. Gómez-Gardenes, Y. Moreno, and A. Arenas, Nonperturbative heterogeneous mean-field approach to epidemic spreading in complex networks, *Physical Review E* **84**, 036105 (2011).
 [19] J. P. Unsleber and M. Reiher, The exploration of chemical reaction networks, *Annual Review of Physical Chemistry* **71**, 121 (2020).

[20] M. Doi, Second quantization representation for classical many-particle system, *Journal of Physics A: Mathematical and General* **9**, 1465 (1976).
 [21] L. Peliti, Path integral approach to birth-death processes on a lattice, *Journal de Physique* **46**, 1469 (1985).
 [22] J. Elser, R. Sterner, E. Gorokhova, W. Fagan, T. Markow, J. Cotner, J. Harrison, S. Hobbie, G. Odell, and L. Weider, Biological stoichiometry from genes to ecosystems, *Ecology Letters* **3**, 540 (2000).
 [23] R. W. Sterner and J. J. Elser, Ecological stoichiometry: the biology of elements from molecules to the biosphere, in *Ecological Stoichiometry* (Princeton University Press, 2017).
 [24] M. F. Weber and E. Frey, Master equations and the theory of stochastic path integrals, *Reports on Progress in Physics* **80**, 046601 (2017).
 [25] V. Elgart and A. Kamenev, Classification of phase transitions in reaction-diffusion models, *Physical Review E* **74**, 041101 (2006).
 [26] A. J. Black and A. J. McKane, WKB calculation of an epidemic outbreak distribution, *Journal of Statistical Mechanics: Theory and Experiment* **2011**, P12006 (2011).
 [27] E. D. Giuli and C. Scalliet, Dynamical mean-field theory: from ecosystems to reaction networks, *Journal of Physics A: Mathematical and Theoretical* **55**, 474002 (2022).
 [28] A. Acín, J. I. Cirac, and M. Lewenstein, Entanglement percolation in quantum networks, *Nature Physics* **3**, 256 (2007).
 [29] G. D. Paparo and M. A. Martin-Delgado, Google in a quantum network, *Scientific Reports* **2**, 444 (2012).
 [30] M. Faccin, T. Johnson, J. Biamonte, S. Kais, and P. Migdal, Degree distribution in quantum walks on complex networks, *Physical Review X* **3**, 041007 (2013).
 [31] M. Faccin, P. Migdal, T. H. Johnson, V. Bergholm, and J. D. Biamonte, Community detection in quantum complex networks, *Physical Review X* **4**, 041012 (2014).
 [32] M. De Domenico, V. Nicosia, A. Arenas, and V. Latora, Structural reducibility of multilayer networks, *Nature Communications* **6**, 6864 (2015).
 [33] M. De Domenico and J. Biamonte, Spectral entropies as information-theoretic tools for complex network comparison, *Physical Review X* **6**, 041062 (2016).
 [34] X. Meng, J. Gao, and S. Havlin, Concurrence percolation in quantum networks, *Physical Review Letters* **126**, 170501 (2021).
 [35] P. Villegas, T. Gili, G. Caldarelli, and A. Gabrielli, Laplacian renormalization group for heterogeneous networks, *Nature Physics* **19**, 445 (2023).
 [36] A. Ghavasiyeh and M. De Domenico, Diversity of information pathways drives sparsity in real-world networks, *Nature Physics*, 1 (2024).
 [37] K. Itakura, J. Ohkubo, and S. ichi Sasa, Two langevin equations in the doi-peliti formalism, *Journal of Physics A: Mathematical and Theoretical* **43**, 125001 (2010).
 [38] O. Artime, N. Khalil, R. Toral, and M. San Miguel, First-passage distributions for the one-dimensional Fokker-Planck equation, *Physical Review E* **98**, 042143 (2018).
 [39] M. Assaf and B. Meerson, WKB theory of large deviations in stochastic populations, *Journal of Physics A: Mathematical and Theoretical* **50**, 10.1088/1751-8121/aa669a (2017).
 [40] B. P. B. A, P. P, and S. A, Mixture distributions in a stochastic gene expression model with delayed feedback:

- a wkb approximation approach, *Journal of Mathematical Biology*, 343 (2020).
- [41] A. Lefèvre and G. Biroli, Dynamics of interacting particle systems: stochastic process and field theory, *Journal of Statistical Mechanics: Theory and Experiment* **2007**, P07024 (2007).
- [42] V. Elgart and A. Kamenev, Rare event statistics in reaction-diffusion systems, *Physical Review E* **70**, 041106 (2004).
- [43] N. Goldenfeld, *Lectures on phase transitions and the renormalization group* (CRC Press, 2018).
- [44] J. Moser and E. J. Zehnder, *Notes on Dynamical Systems* (American Mathematical Society, 2005).
- [45] N. Van Kampen, *Stochastic Processes in Physics and Chemistry* (Elsevier, Amsterdam, 2007) 3rd ed.
- [46] O. Artime, A. Carro, A. F. Peralta, J. J. Ramasco, M. San Miguel, and R. Toral, Herding and idiosyncratic choices: Nonlinearity and aging-induced transitions in the noisy voter model, *Comptes Rendus Physique* **20**, 262 (2019).
- [47] K. Huang, *Statistical Mechanics* (John Wiley & Sons, 1987).
- [48] R. Sole, Nonequilibrium dynamics in conservation biology: Scales, attractors and critical points, Preprints [10.20944/preprints202310.1646.v1](https://arxiv.org/abs/10.20944/preprints202310.1646.v1) (2023).
- [49] A. Barrat, M. Barthélemy, and A. Vespignani, *Dynamical Processes on Complex Networks* (Cambridge University Press, 2008).
- [50] P. D. Hines, I. Dobson, and P. Rezaei, Cascading power outages propagate locally in an influence graph that is not the actual grid topology, *IEEE Transactions on Power Systems* **32**, 958 (2016).
- [51] L. Xing, Cascading failures in internet of things: review and perspectives on reliability and resilience, *IEEE Internet of Things Journal* **8**, 44 (2020).
- [52] R. M. May, Will a large complex system be stable?, *Nature* **238**, 413 (1972).
- [53] S. Allesina and S. Tang, Stability criteria for complex ecosystems, *Nature* **483**, 205 (2012).
- [54] G. Bunin, Ecological communities with Lotka-Volterra dynamics, *Physical Review E* **95**, 042414 (2017).
- [55] S. Allesina and S. Tang, The stability–complexity relationship at age 40: a random matrix perspective, *Population Ecology* **57**, 63 (2015).
- [56] G. Biroli, G. Bunin, and C. Cammarota, Marginally stable equilibria in critical ecosystems, *New Journal of Physics* **20**, 083051 (2018).
- [57] F. Roy, M. Barbier, G. Biroli, and G. Bunin, Complex interactions can create persistent fluctuations in high-diversity ecosystems, *PLoS Computational Biology* **16**, e1007827 (2020).
- [58] P. Van den Driessche and J. Watmough, Reproduction numbers and sub-threshold endemic equilibria for compartmental models of disease transmission, *Mathematical Biosciences* **180**, 29 (2002).
- [59] F. Battiston, E. Amico, A. Barrat, G. Bianconi, G. Ferraz de Arruda, B. Franceschiello, I. Iacopini, S. Kéfi, V. Latora, Y. Moreno, *et al.*, The physics of higher-order interactions in complex systems, *Nature Physics* **17**, 1093 (2021).
- [60] M. Shimada, P. Behrad, and E. D. Giuli, Universal slow dynamics of chemical reaction networks (2024), [arXiv:2304.10072 \[q-bio.MN\]](https://arxiv.org/abs/2304.10072).
- [61] G. W. A. Constable, A. J. McKane, and T. Rogers, Stochastic dynamics on slow manifolds, *Journal of Physics A: Mathematical and Theoretical* **46**, 295002 (2013).
- [62] A. Barrat, M. Barthelemy, and A. Vespignani, *Dynamical processes on complex networks* (Cambridge University Press, 2008).
- [63] N. Crokidakis, A simple mechanism leading to first-order phase transitions in a model of tax evasion, *International Journal of Modern Physics C* **33**, [10.1142/s0129183122500759](https://doi.org/10.1142/s0129183122500759) (2021).